NTNU – Trondheim
Norwegian University of
Science and Technology

Analysis of ROV Lift Operation

Runa Folvik Bjerkholt

Marine Technology
Submission date: June 2014
Supervisor: Svein Sævik, IMT
Co-supervisor: Dag Abel Sveen, DeepOcean

Norwegian University of Science and Technology
Department of Marine Technology

NTNU Trondheim
Norges teknisk-naturvitenskapelige universitet
Institutt for marin teknikk

MASTER THESIS 2014

for

Stud. tech. Runa Folvik Bjerkholt

ANALYSIS OF ROV LIFT OPERATION

Analyse av ROV løfteoperasjon

The background for this project is related to ROV offshore operations where water entry represents of the most critical design scenarios limiting the H_s operation window. Using relevant standards together with analytical calculations will include inherent conservatism. The focus of this project work is to investigate the conservatism by computational methods and the variability between different tools. The project work is to be carried out as follows:

1. Literature study, including relevant standards for lift operations, and the basic principles applied in computational tools like Orcaflex and Simo/Riflex.
2. Define an ROV lift scenario and perform analytical calculations based on the standard methods. Define the basis for parameter variation.
3. Establish computational models in Orcaflex and SIMA(Simo/Riflex)
4. Demonstrate the performance of the models.
5. Perform parameter variation using both models.
6. Compare results obtained by the computational models with reference to the analytical result.
7. Conclusions and recommendations for further work

All necessary input data is assumed to be provided by DeepOcean, so also the Orcaflex license.

The work scope may prove to be larger than initially anticipated. Subject to approval from the supervisors, topics may be deleted from the list above or reduced in extent.

In the thesis the candidate shall present her personal contribution to the resolution of problems within the scope of the thesis work

Theories and conclusions should be based on mathematical derivations and/or logic reasoning identifying the various steps in the deduction.

The candidate should utilise the existing possibilities for obtaining relevant literature.

Thesis format
The thesis should be organised in a rational manner to give a clear exposition of results, assessments, and conclusions. The text should be brief and to the point, with a clear language. Telegraphic language should be avoided.

The thesis shall contain the following elements: A text defining the scope, preface, list of contents, summary, main body of thesis, conclusions with recommendations for further work, list of symbols and acronyms, references and (optional) appendices. All figures, tables and equations shall be numerated.

The supervisors may require that the candidate, in an early stage of the work, present a written plan for the completion of the work.

The original contribution of the candidate and material taken from other sources shall be clearly defined. Work from other sources shall be properly referenced using an acknowledged referencing system.

The report shall be submitted in two copies:

- Signed by the candidate
- The text defining the scope included
- In bound volume(s)
- Drawings and/or computer prints which cannot be bound should be organised in a separate folder.

Ownership
NTNU has according to the present rules the ownership of the thesis. Any use of the thesis has to be approved by NTNU (or external partner when this applies). The department has the right to use the thesis as if the work was carried out by a NTNU employee, if nothing else has been agreed in advance.

Thesis supervisors:

Prof. Svein Sævik, NTNU
Dag Abel Sveen, DeepOcean

Deadline: June 10th 2014

Trondheim, January, 2014

Svein Sævik

Preface

This master thesis has been carried out in the spring of 2014. The thesis is the final step to fulfil the requirements of the degree Master of Science in Marine Technology. The work performed in this thesis is a continuation of the project work carried out in the autumn of 2013. It is written in cooperation with DeepOcean.

The main objective has been to investigate an ROV lift operation through the splash zone. Analytical calculations have been performed according to relevant standards. In addition, computational models of the ROV lift operation has been conducted in the two software programs SIMA and OrcaFlex. At the earliest stage of the thesis work a considerable amount of time was put into an additional scope of capturing the shielding effect from the vessel with the use of diffraction programs like WADAM or WAMIT. This proved to be a challenge due to the lack of data needed, and the focus was turned to the above-mentioned scope.

Prior to the thesis I had no knowledge of the simulation programs OrcaFlex and SIMA/SIMO or the programming language Python. A large amount of time has therefore been used to achieve this knowledge. The modelling, automation and post processing of the results have been a demanding and time consuming process, but also very educational.

I would especially like to thank my supervisor at NTNU, Svein Sævik for useful discussions, guidance and taking the time to answer my questions throughout the semester. In addition, I would like to thank my supervisor at DeepOcean Dag Abel Sveen, for proposing the topic of this master thesis. He has provided me with the initial spread sheet for performing the analytical calculations and valuable input for the software programs. He also proposed to send me to Aberdeen to attend a two-day training course in OrcaFlex. The course was very valuable to achieve a better understanding of the programme. Orcina has also been of great help for setting up the automation of the simulations in OrcaFlex and helping me with other difficulties in OrcaFlex. I also wish to thank Knut Mo and Andreas Amundsen at MARINTEK for helping me out with questions regarding SIMA/SIMO.

Trondheim, 10-06-2014

Runa Folvik Bjerkholt

Summary

As a service company performing subsea operations, DeepOcean wishes to operate in the widest range of sea conditions. The majority of all offshore operations are performed using remotely operated vehicles (ROVs), where lifting through the splash zone is considered the most critical phase during launching and recovery of the ROV system. Available standards from DNV propose a systematic and analytical approach for estimating the hydrodynamic loads occurring in the splash zone. A maximum operational significant wave height, H_s, is determined using a proposed acceptance criteria. Experience from the industry have shown that the method is unreasonable conservative, consequently leading to a restrictive operational H_s window.

The main objective of this master thesis is to compare results obtained from the analytical calculations with results obtained from the time domain simulation programs; Simulation of Marine Operations (SIMO) and OrcaFlex. The operational limit established in the time domain programs is based on the assumption that the maximum relative velocity between the crane tip and the waves represent a worst case scenario and that a slack lifting wire is not acceptable. This is due to the uncertainties associated with snap loading after a slack lifting wire. Three different ROV models have been established, two in OrcaFlex and one in SIMO. A sensitivity study regarding the hydrodynamic coefficients for the ROV models is also performed.

The three different ROV models show different dependency of the added mass and drag term. The overall trend for the ROV systems is that the added mass dependency is reduced for the structures modelled with multiple elements, while the drag dependency is increased.

The Simplified Method is certainly conservative compared to time domain simulations performed in SIMO and OrcaFlex. The present operational sea state of H_s = 4.5 m is rejected by the Simplified Method. If the operation is to be performed independent of a T_s value, an operational H_s of 0.75 m is acceptable according to the analytical calculations. From the time domain analyses in SIMO and OrcaFlex, the current operational sea state of H_s = 4.5 m could be justified if a limiting T_z is given. For launching this limiting value is 9 s, while for recovery of the ROV system the limiting T_z value is 8 s. The operational limit should not only be set by a H_s value, but also a T_z due to the large dependency of the wave period for lifting though the splash zone. Simulating the ROV lift operation in a time domain simulation program has proven to be a good alternative compared to the Simplified Method.

Sammendrag

Som et serviceselskap som utfører undervannsoperasjoner, ønsker DeepOcean å operere i et størst mulig spekter av sjøtilstander. De fleste offshoreoperasjoner er utført ved hjelp av fjernstyrte undervannsfartøy (ROV). Løfting av ROVen gjennom skvalpesonen regnes som den mest kritiske fasen av operasjonen på grunn av store rykklaster som kan oppstå i løftevaieren. Anbefalt praksis fra DNV foreslår en systematisk og forenklet metode for å beregne kreftene som oppstår på det løftede legemet i skvalpesonen. En maksimal operativ signifikant bølgehøyde, H_s, blir bestemt av et gitt akseptkriterium. Erfaringer fra bransjen har vist at metoden er urimelig konservativ, noe som betyr at det tillatte operasjonelle vinduet blir svært lite.

Hovedmålet med denne masteroppgaven er å sammenligne resultatene fra de analytiske beregningene med resultatene fra analyseprogrammene; Simulation of Marine Operations (SIMO) og OrcaFlex. Det operasjonelle vinduet i analyseprogrammene er bestemt ut i fra antagelsen om at den maksimale relative hastigheten mellom krantuppen og bølgen representerer det verst tenkelige tilfellet og at en slakk løftevaier ikke er akseptabelt. Tre ulike ROV modeller har blir analysert, to i OrcaFlex og en i SIMO. De hydrodynamiske koeffisientene definert for ROVene har blitt studert for å se hvordan dette påvirker resultatene.

De tre ROVmodellene viser forskjellig avhengighet av tilleggsmasse og drag. Påvirkningen av tilleggsmasse blir redusert for modellene med flere elementer, mens påvirkningen fra drag øker.

Slik som erfaringene fra bransjen tilsier, er den forenklede metoden fra DNV konservativ. Dagens operasjonell H_s = 4.5 m blir ikke godkjent av det gitte akseptkriteriet. Dersom løfteoperasjonen skal kunne utføres uavhengig av T_z verdi, er H_s = 0.75 m akseptabelt. Fra analyseprogrammene kan den gjeldende operasjonelle H_s = 4.5 m kunne forsvares dersom en begrensende T_z verdi er gitt. For sjøsetting er begrensningen 9 s, og for løfting er begrensningen 8 s. Siden kreftene som oppstår i skvalpesonen er høyst avhengig av T_z periode, bør det tillatte operasjonelle vinduet bli satt med en slik begrensning, ikke bare med operasjonell H_s. Simulering av løfteoperasjonen med analyseverktøy som SIMO og OrcaFlex har vist seg å være ett godt alternativ til den forenklede metoden.

Contents

List of Figures

List of Tables

Nomenclature

Abbreviations

AP	Aft Perpendicular
COG	Centre of Gravity
DNV	Det Norske Veritas
DOF	Degrees Of Freedom
GM_L	Longitudinal metacentric height
GM_T	Transverse metacentric height
HF	High Frequency
IMR	Inspection, Maintenance, Repair
KC	Keulegan-Carpenter
LARS	Launch and Recovery System
LF	Low Frequency
OBS-ROV	Observation ROV
RAO	Response Amplitude Operator
ROV	Remotely Operated Vehicle
SIMO	Simulation of Marine Operations
TMS	Tether Management System
W-ROV	Work ROV

Roman Symbols

$\tilde{A}_w$	Water line area of object
A_{33i}	Added mass in heave of the substructure
A_{33}	Added mass in heave

A_{33}^{∞}	High-frequency limit heave added mass
A_p	Horizontal projected area of object
A_s	Slamming area
a_w	Vertical water particle acceleration
B_1	Linear damping
b_1	Non-dimensional linear damping coefficient
B_2	Quadratic damping
b_2	Non-dimensional quadratic damping coefficient
B_{crit}	Critical damping
C	Correction factor
C_a	Added Mass coeffiecient
C_{ds}	Steady state drag coeffiecient
C_e	Water exit coefficient
C_s	Drag coeffiecient
C_s	Slamming coeffiecient
D	Diameter
d	Distance from the centre of gravity of submerged part to water plane
F_{hydro}	Hydrodynamic force
F_{static}	Static force of lifted object
F_{B1}	Linear damping force
F_{B2}	Quadratic damping force
F_B	Buoyancy force
F_{Di}	Drag force on substructure
F_E	Water exit force
F_H	Hydrodynamic force
F_{Mi}	Mass force on substructure

F_M	Mass force
$F_{slender}$	Water exit force
F_{snap}	Snap Force
F_S	Slamming force
F_W	Wave force
g	Acceleration of gravity
h	Submergence relative to the water plane
H_s	Significant wave height
K	Stiffness
k_0	Flexibility of crane
M	Mass of object
M_i	Mass of substructure
M_s	Structural mass
$S_J(\omega)$	JONSWAP-spectrum
$S_{PM}(\omega)$	Pierson-Moskowitz spectrum
T	Wave period
T_p	Peak period
T_z	Zero-up-crossing wave period
V	Volume of displaced water
v_{ff}	Free fall velocity
v_{snap}	Snap velocity
v_s	Slamming velocity
v_w	Vertical water particle velocity
W	Submerged weight of object
W_0	Weight in of object in air
$\ddot{x}_r$	Relative vertical acceleration

$\ddot{x}$	Vertical acceleration of object
$\dot{x}_r$	Relative vertical velocity
$\dot{x}$	Vertical velocity of object
z	Distance to water surface

Greek Symbols

δV	Time dependent volume
η_{ct}	Amplitude of the vertical motion of the crane tip
γ	Peak shape parameter
ω'	Non-dimensional oscillation frequency
ω_p	Spectral peak frequency
ρ	Density of salt water
σ	Spectral width parameter
ζ_a	Wave amplitude
A_γ	Normalizing factor

1 Introduction

1.1 Background and Motivation

As a service company performing subsea operations, DeepOcean wishes to operate in the widest range of sea conditions. Reducing operational downtime is an important aspect of keeping the company competitive in the market and limiting the costs associated with marine operations.

The majority of all offshore operations are performed using remotely operated vehicles (ROVs). Lifting through the splash zone is considered the most critical phase during launching and recovery of the ROV-system. During this phase of the operation the lifting wire may become slack due to the hydrodynamic forces acting on the lowered object in the splash zone. A slack lifting wire should to all extent be avoided due to the uncertainties associated with snap loading after the lifting wire undergoes goes slack.

The recommended practice from DNV "Modelling and Analysis of Marine Operation", (DNV, 2011) proposes a systematic and analytical approach for estimating the hydrodynamic loads occurring in the splash zone. A maximum operational significant wave height, H_s, is determined using a proposed acceptance criteria. Experience from the industry have shown that the method is unreasonable conservative, consequently leading to a restrictive operational H_s window. The Recommended Practice from DNV allows for other approaches of determining an operational sea state for lifting though the splash zone. Modelling and simulating the lifting operation in a time domain computer program is an alternative to the systematic approach proposed by DNV.

1.2 Objective

The main objective of this master thesis is to compare results obtained from the analytical calculations with results obtained from the time domain simulation programs; Simulation of Marine Operations (SIMO) and OrcaFlex. The challenge of interest is to determine an operational window from the analytical calculations and the time domain simulations for comparison. In addition, a sensitivity study of the computational models is addressed.

1.3 Previous Work

Considerable amounts of published work addresses the problem of lowering objects through the splash zone. Sarkar and Gumestad (2010) have performed a detailed discussion of the recommended practice "Modelling and Analysis of Marine Operation" DNV (2011) where the focus is on the hydrodynamic coefficients and the methodology suggested for analysis of lifting operations through the splash zone. Kopsov and Sandvik (1995) present a study where experimental and theoretical approaches are used to establish a design and operational criteria for the main installation stages of subsea structures. Øritsland and Lehn (1987) have presented a comprehensive study of the hydrodynamic coefficients of idealized subsea structures. Numerous model tests are performed, and in Øritsland (1989) a total summary of the hydrodynamic coefficients of different subsea structures may be found. Thurson et al. (2011) have investigated the nonlinear dynamic tension in the lifting wire due to snap loads.

1.4 Scope and Limitations

Due to the large nonlinearities present in the splash zone, the use of linear wave theory is strictly speaking not applicable for the analyses performed in this thesis. The use of linear wave theory to describe irregular waves is therefore a simplification of the environment.

Although wind and current are environmental parameters most likely to be present at the time of the lifting operation, these effects have not been taken into account. The wind may cause excessive pendulum motion of the ROV system in air, but the vertical motion of the system is assumed to dominate the lifting operation. A current may cause additional hydrodynamic forces on the system, but is neglected in the splash zone.

The motion of the vessel is only described by first order transfer functions, implying that the presence of the vessel in the waves is not captured. This includes shielding effect from the vessel when performing the lowering operation on leeward side, and radiation effects due to the oscillation of the vessel in waves.

The ROV models used in this thesis are based on drawings and main dimensions received from DeepOcean. The models therefore represent a simplification of the real ROV system and may therefore lead to deviations in the results.

For some sea states the dynamic tension after a slack lifting wire occurs may be within the acceptable structural design limit for the lifting wire. Nevertheless, due to the uncertainties associated with snatch loading, the operational window for the ROV lift operation is limited by the sea states that induce a slack lifting wire. Hence, snap loading is not considered in detail.

1.5 Structure of the Report

The vessel, lifting and ROV system used in this thesis is described in Chapter 2. This is the basis for the input used in the analytical calculations and in the time domain simulations.

Chapter 3 presents the literature review of lifting though the splash zone and the Simplfied Method as outlined in DNV (2011), which is used in the analytical calculations. In addition, a section describing and determining the hydrodynamic coefficients is provided. The theory of the two software programs used is described in Chapter 4.

The methodology chapter, Chapter 5, outlines how the analytical calculations are performed and addresses the modelling and analyses of the system in SIMO and OrcaFlex. An additional section is included where a validation of the modelling is performed.

Chapter 6 presents the results obtained from the analytical calculations and the time-domain simulations. The interpretations and discussion of the results obtained from the analytical calculations and the time domain programs are outlined in Chapter 7.

The two last chapters address the conclusion of this thesis and recommendations for further work.

2 Description of system

2.1 Edda Flora

Edda Flora is a service vessel for subsea operations. It is especially designed to perform inspection, maintenance and repair (IMR) work of installations situated below the sea surface. The main characteristics of the vessel are presented in Table 2.1. The first order transfer function for Edda Flora is calculated by Skipsteknisk (Lien, 2009). The vertical centre of gravity, VCG, is defined from aft perpendicular (AP), and the longitudinal centre of gravity, LCG, is taken as distance above the keel.

Figure 2.1: Edda Flora

Table 2.1: Main dimensions of Edda Flora

Main Dimansions	Value	Unit
Lpp	82.20	[m]
Loa	95.00	[m]
Breadth	20.00	[m]
Mean draught	6.48	[m]
Deadweight	2442	[Te]
Lightweight	4244	[Te]
Displacement	6686	[Te]
VCG	8.59	[m]
LCG	38.36	[m]

2.2 ROV, TMS and Lifting system

The vessel is equipped with two Supporter W-ROV's and one V8 Offshore OBS-ROV. The ROVs are either used for observation (OBS-ROV) or for working (W-ROV). They are linked to the mother vessel, Edda Flora by an umbilical cable. The umbilical cable is managed by the tether management system (TMS), which holds the umbilical drum. After the whole system has been lowered through the splash zone, the TMS is stationed some meters below the sea surface. The ROV is then disconnected and free to move with only the umbilical as a connection to the TMS. In this thesis, the properties of the Supporter ROV are applied. The main dimensions of the ROV and TMS are found in Table 2.2 and 2.3, where the mass of the ROV includes skid manipulators. As seen from Table 2.2 the ROV is neutrally buoyant in water. The present operational limit as of today for the Supporter ROV is 4.5m.

Table 2.2: ROV Supporter - Main dimensions

Main Dimensions	Value	Unit
Length	2.50	[m]
Width	1.70	[m]
Height	1.65	[m]
Displacement	3.46	[m^3]
Mass	3.55	[Te]
Weight	34.83	[kN]
Weight in water	0.00	[kN]

Table 2.3: TMS - Main dimensions

Main Dimensions	Value	Unit
Diameter	1.70	[m]
Height	1.30	[m]
Displacement	0.78	[m^3]
Mass	3.50	[Te]
Weight	34.34	[kN]
Weight in water	26.53	[kN]

Figure 2.2: ROV - Supporter

The ROV system is launched and recovered by an A-frame (LARS). The crane tip is positioned 42.8 m in front of AP, 12 m from the centre line and 13.2 m above the keel. It is assumed that the stiffness of the A-frame has a linear relationship between the force deflection δ. The stiffness of LARS is 3330 kN/m. The hoisting umbilical, used for lowering the ROV system, is of steel armour with properties given in Table 2.4. LARS and umbilical properties are obtained from DeepOcean.

Table 2.4: Properties of the umbilical

Dimensions	Value	Unit
Outer diameter	32.6	[mm]
Mass/unit length	3.50	[kg/m]
Mass in seawater/unit length	2.70	[kg/m]
Axial stiffness	30 000	[kN]

3 Lifting Through the Splash Zone

Lifting through the splash zone is a complex hydrodynamic problem. The following section describes the complete problem of lifting through the splash zone. In addition the simplified approach for analytical calculations of the problem proposed in the DNV Recommended Practice "Modelling and Analysis of Marine Operation" (DNV, 2011) is elaborated. A deliberation of the hydrodynamic coefficients of the ROV system is also included in this section.

3.1 Lifting Operation

A subsea lifting operation may be divided into four main phases:

- Lift off from deck
- Lowering through the splash zone
- Lowering to sea bed
- Landing on sea bed

In most lifting operations, lowering through the splash zone is considered as the most critical phase of a subsea lifting operations. A lifting operation may be divided into a heavy lift and a light lift operation. In a heavy lift operation, the weight of the lifted object is more than 1-2 % of the vessel's displacement. In a light lift operation the lifted object is less than 1-2 % of the displacement of the vessel, and the lifted object does not affect the vessel motions (DNV, 2011). The ROV lift operation investigated in this thesis is a light lift operation.

A light lift operation allows the crane to be modelled as stiff and the motions of the crane tip can be determined from the vessel's transfer functions of the body motions, also named the response amplitude operators (RAO). They are defined as response amplitude per unit wave amplitude. The RAOs are given in six degrees of freedom and defined at the vessel's centre of gravity (COG). The motion RAOs are used together with the position of the crane tip to define the wave induced translational motion of the crane tip.

3.2 Environment

The sea elevation is described statistically based on random process theory. Long-crested irregular waves are described as a sum of linear regular waves. Figure 3.1, modified from Figure 2.1 from Faltinsen (1990), shows the wave profile of a regular wave, the corresponding vertical component of the water particle velocity and the vertical component of the water particle acceleration. The maximum for each component occur at different time instants as the components have different phase angles. This is further used in Section 5.1.3. The vertical velocity and acceleration of a regular propagating wave is given by the two following equation:

$$v_w = \frac{2\pi}{T}\zeta_a e^{kz}\cos(\omega t - kx) \tag{3.1}$$

$$a_w = (\frac{2\pi}{T})^2\zeta_a e^{kz}\sin(\omega t - kx) \tag{3.2}$$

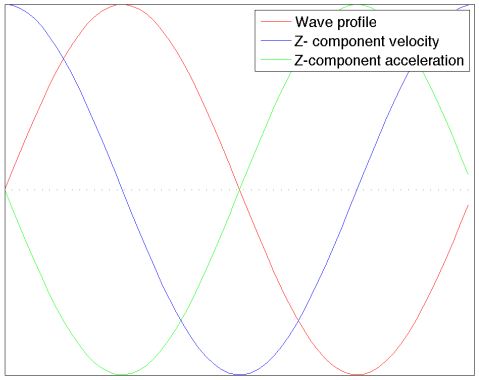

Figure 3.1: Wave profile, velocity and acceleration of a wave

For a random wave analysis, the JONSWAP-spectrum is used to describe the sea state. This spectrum is representative for the sea conditions that occur in the North Sea. The JONSWAP-spectrum is described by 5 parameters, and is based on the Pierson-Moskowitz (PM) spectrum (DNV, 2010). The JONSWAP-spectrum is given by the following equation:

$$S_J(\omega) = A_\gamma S_{PM}(\omega)\gamma^{e^{(-0.5(\frac{\omega-\omega_p}{\sigma\omega})^2)}} \tag{3.3}$$

Where the PM-spectrum is given as:

$$S_{PM}(\omega) = \frac{5}{16}H_s^2\omega_p^4\omega^{-5}e^{-\frac{5}{4}(\frac{\omega}{\omega p})^{-4}} \tag{3.4}$$

where
A_γ = 1-0.287ln(γ), normalizing factor

γ = peak shape parameter
$\omega_p = \frac{2\pi}{T_p}$, spectral peak frequency
T_p = peak period
σ = spectral width parameter
$\sigma = \sigma_a$ for $\omega \leq \omega_p$
$\sigma = \sigma_b$ for $\omega > \omega_p$
Average values for the parameters are $\gamma = 3.3$, $\sigma_a = 0.07$ and $\sigma_b = 0.09$.

T_z is related to T_p by the following relation:

$$\frac{T_z}{T_p} = 0.6673 + 0.05037\gamma - 0.006230\gamma^2 + 0.0003341\gamma^3 \tag{3.5}$$

For $\gamma = 3.3$, the ratio between the T_p and T_z is:

$$\frac{T_p}{T_z} = 1.2843 \tag{3.6}$$

The relevant T_z values and the corresponding T_p values are listen in Table 3.1.

Table 3.1: Peak and zero up-crossing period

T_z [s]	5	6	7	8	9	10	11	12	13
T_p [s]	6.42	7.71	8.99	10.27	11.56	12.84	14.13	15.41	16.70

In a long term description of the sea state the significant wave height and mean wave period will vary. A scatter diagram representative for the northern North Sea (Faltinsen, 1990) is included in Appendix B. The scatter diagram shows the joint frequency between H_s and T_p and may be used to find the probability of a H_s value occurring given a certain T_p value or the probability a T_p value being less than a specific value, given a H_s.

For a given significant wave height, H_s the following zero-up-crossing wave period range T_z, should be considered. The acceleration of gravity is denoted g.

$$8.9\sqrt{\frac{H_s}{g}} \leq T_z \leq 13 \tag{3.7}$$

If the lifting operation is to be performed independent of vessel heading, the vessel response should be analysed for wave directions at least $\pm 15\,^\circ$ off vessel heading.

3.3 Loads in the Splash Zone

A structure that is being lowered through the splash zone is exposed to a number of different forces and the problem is highly non-linear. Accurate prediction of these forces may reduce downtime of the operational vessel and increase the safety of the operation. The following section describes the forces occurring in the splash zone with reference to DNV (2011).

3.3.1 Weight of Structure

The hydrostatic buoyancy of the structure W is obtained by combining the weight of the structure in air W_0 and the buoyancy force F_B. The two forces counteract each other, causing the submerged weight of the object to be reduced compared to the weight of the object in air.

$$W = W_0 - F_B = M_s - \rho V g \tag{3.8}$$

M_s represents the structural mass of the object, V is the submerged volume of the object, ρ is the density of salt water and g is the acceleration of gravity.

3.3.2 Hydrodynamic Forces

The hydrodynamic loads occurring in the splash zone originate from Faltinsen's description of linear dynamic loads and motions of structures in regular waves (Faltinsen, 1990). The loads may be divided into two problems:

- Radiation problem
- Wave excitation problem

The radiation problem is solved by forcing the structure to oscillate in six degrees of freedom. There are no incident waves in this problem, and the moving body generates radiated waves due to the forced oscillation. The hydrodynamic loads in the radiation problem are the added mass, damping and restoring forces. The excitation problem consists of the Froude-Kriloff and diffraction forces. Restraining the structure from oscillatory motion, and allowing incoming regular waves to interact with the object solves the excitation problem. The Froude-Kriloff forces represent the forces acting on the structure as if the structure is not present, and the diffraction forces recover impermeability and cause a flow due to the presence of the structure. Due to linearity the two problems may be added together as the hydrodynamic force F_H. The total equation of motion in the vertical direction then takes the following form (Øritsland and Lehn, 1989):

$$F_H + W + F_L = M\ddot{x} \tag{3.9}$$

By assuming that the body is small compared to the wave length, the wave diffraction force generated by the body may be neglected. A consequence of this assumption may be that the lift line force F_L is too conservative. This is often seen for sea states with short waves (Kopsov and

Sandvik, 1995). According to the Recommended Practice (DNV, 2011) a slack lifting wire should to all extent be avoided as this may lead to large snatch forces.

The radiation force F_R, is dependent on the object velocity $\dot{x}$ and acceleration $\ddot{x}$. Due to the proximity to the free surface the hydrodynamic forces are dependent on the distance to the free surface (Sandvik et al., 1993).

$$F_R = \frac{d}{dt}(M\dot{x}) + B_1\dot{x} + B_2\dot{x}\,|\,\dot{x}\,| \tag{3.10}$$

The mass variation with time is rewritten as:

$$\begin{aligned} \frac{d}{dt}(M\dot{x}) &= M\ddot{x} + \frac{dM}{dt}\dot{x} \\ &= M\ddot{x} + \frac{dA_{33}}{dt}\dot{x} \\ &= M\ddot{x} + \frac{dA_{33}}{dh}\frac{dh}{dt}\dot{x} \end{aligned} \tag{3.11}$$

The first term is the inertia term and the last term expresses the dependency of the immersion of the object. It is associated with the slamming force, and acting in the upward direction. M is the sum of the structural mass and the added mass, where the added mass is expressed by a depth dependent added mass coefficient. The distance to the free surface is denoted h.

$$\begin{aligned} M &= M_s + A_{33} \\ &= M_s + \rho V C_a \end{aligned} \tag{3.12}$$

For Keulegan-Carpenter (KC) number less than 10, which is the case for most lifting operations, it is convenient to express the drag and damping as a sum of a linear and a quadratic term, B_1 and B_2. These terms are further described in Section 3.5.2.

The wave forces F_W, depend on the water particle velocity v_w and acceleration a_w.

$$\begin{aligned} F_W &= \rho V a_w + \frac{d}{dt}(A_{33}v_w) + F_D \\ &= (\rho V + A_{33})a_w + \frac{dA_{33}}{dh}\frac{dh}{dt}a_w + F_D \end{aligned} \tag{3.13}$$

The first term of the wave force is the pressure gradient due to the waves and the second term is the change in fluid momentum. This force is also associated with the slamming force. F_D is the hydrodynamic drag (or damping) and is expressed in the same manner as the damping terms in Equation 3.10, but dependent of the water particle velocity v_w.

The total hydrodynamic force is obtained by combining the body reaction force and the wave force. Introducing the vertical relative velocity between the object and the water particles gives

the total equation of motion (Øritsland and Lehn, 1989):

$$\underbrace{(M_s + A_{33})\ddot{x}}_{\text{Inertia force}} = \underbrace{B_1 v_r}_{\text{Linear damping}} + \underbrace{B_2 v_r \mid v_r \mid}_{\text{Quadratic damping}} + \underbrace{(\rho V + A_{33}) a_w}_{\text{Wave forces}} + \underbrace{\frac{dA_{33}^{\infty}}{dt} v_r}_{\text{Slamming}} - \underbrace{W}_{\text{Weight}} + \underbrace{F_L(t)}_{\text{Line force}} \tag{3.14}$$

The added mass term A_{33}^{∞} in the slamming expression is the high-frequency limit added mass, which assumes that the water particle accelerations due to the slamming effect are much larger than the acceleration of gravity. This is further discussed in Section 3.5.4

The slamming force F_S, may also be expressed in terms of a slamming coefficient. The slamming coefficient is further discussed in Section 3.5.

$$F_S = \frac{1}{2}\rho C_s A_p v_r^2 \tag{3.15}$$

In the same manner as the slamming force, the water exit force may also be expressed as a function of a water exit coefficient C_e.

$$F_E = -\frac{1}{2}\rho C_e A_p v_r^2 \tag{3.16}$$

3.4 Simplified Method

The following section describes the Simplified Method as outlined in DNV-RP-H103 "Modelling and Analysis of Marine Operations'"(DNV, 2011). The method gives a simplifed and conservative approach to calculate the hydrodynamic loads described in Section 3.3. This method forms the basis for the analytical calculations performed in this thesis.

The Simplified Method is based on three main assumptions in order to be valid. It assumes that the horizontal extent of the object that is being deployed is small compared to the wave length. This assumption allows the hydrodynamic loads to be calculated at characteristic points of the structure, and then added together. The second assumption is that the vertical motion of the object follows the motion of the crane tip. At last, it is assumed that the vertical forces dominate the load case.

3.4.1 Wave Kinematics

The operation through the wave zone is assumed to be conducted within 30 minutes (DNV, 2011). With these assumptions, the following wave amplitude, wave particle velocity and wave particle acceleration is valid.

$$\zeta_a = 0.9 H_s \tag{3.17}$$

$$v_w = \zeta_a (\frac{2\pi}{T_z}) e^{-\frac{4\pi^2 d}{T_z^2 g}} \tag{3.18}$$

$$a_w = \zeta_a (\frac{2\pi}{T_z})^2 e^{-\frac{4\pi^2 d}{T_z^2 g}} \tag{3.19}$$

ζ_a is the wave amplitude, v_w is the vertical water particle velocity, and a_w is the vertical water particle acceleration. The parameter d is the distance from the water plane to the COG of the submerged part of the object.

3.4.2 Accept Criteria

The Simplified Method proposes an accept criteria to ensure that the lifting wire is always in tension. The lifting wire may become slack if the upward hydrodynamic loads are larger than the static weight of the lifted object. A conservative estimate is made by ensuring that the acceptable limit of hydrodynamic loads should not exceed 90% of the static weight of the object.

$$F_{\text{hydro}} \leq 0.9 F_{\text{static}} \tag{3.20}$$

3.4.3 Static force

The static force F_{static} in the accept criteria may be recognized as the weight of the lifted object described in Section 3.3.1. The Simplified Method uses the volume of the displaced water relative to the still water surface condition, given for each defined loadcase. The loadcases are defined in Section 5.1.3.

$$F_{\text{static}} = Mg - \rho V g \tag{3.21}$$

3.4.4 Hydrodynamic forces

The varying buoyancy force F_ρ, is caused by the change in the surface elevation and is the same force as the second term in Equation 3.8.

$$F_\rho = \rho \delta V g \tag{3.22}$$

The time-dependent volume from Equation 3.8 is expressed as δV. The change in volume of displaced water is dependent of the water line area $\tilde{A}_w$, the amplitude of the vertical motion of the crane tip η_{ct}, and the wave amplitude.

$$\delta V = \tilde{A}_w \sqrt{\zeta_a^2 + \eta_{ct}^2} \tag{3.23}$$

The Simplified Method allows a complex structure to divided into substructures, where the mass force for each substructure is calculated individually. The mass force for each substructure is then summarized to the total mass force F_M.

$$F_M = \sum_i F_{Mi} \tag{3.24}$$

The inertia force and force contributions from Froude Kriloff forces and diffraction forces make up the mass force. The force arise due to the acceleration of the object and the water particles. It is expressed as:

$$F_{Mi} = \sqrt{[(M_i + A_{33i})a_{ct}]^2 + [(\rho V_i + A_{33i})a_w]^2} \tag{3.25}$$

M_i is the mass of the substructure in air and A_{33i} is the added mass in heave of the substructure. Acceleration of the crane tip and acceleration of the vertical water particle is given by a_{ct} and a_w, respectively.

As for the mass force, the drag force may also be calculated individually for each substructure. The linear and quadratic drag term from Equation 3.14 is simplified to the quadratic drag term of Morison's equation. The drag coefficient C_d is discussed further in section 3.5. A_p is projected area of the submerged part of the object.

$$F_{Di} = 0.5 \rho C_D A_p v_r^2 \tag{3.26}$$

The relative velocity between the objects and the water particles v_r is taken as:

$$v_r = v_c + \sqrt{v_{ct}^2 + v_w^2} \tag{3.27}$$

The lowering velocity of the crane is v_c, v_{ct} is the amplitude velocity of the crane tip and v_w is the vertical water particle velocity. The total drag force may also be summarized in the same manner as the mass force:

$$F_D = \sum_i F_{Di} \tag{3.28}$$

The slamming forces occur during the impact between the object and the water. It is given as:

$$F_S = 0.5\rho C_s A_s v_s^2 \tag{3.29}$$

C_s is the slamming coefficient which is further dicussed in Section 3.5. A_s is the projected area that is subjected to the slamming force and v_s is the impact slamming velocity, which is the same as the relative velocity in Equation 3.27.

The total hydrodynamic force is a function of the slamming force, varying buoyancy force, mass force and the drag force.

$$F_H = \sqrt{(F_D + F_S)^2 + (F_M - F_\rho)^2} \tag{3.30}$$

The force components in the total hydrodynamic force are dependent on the different components of the wave showed in Figure 3.1. The varying buoyancy force is position dependent, the slamming force and the drag force is velocity dependent and the mass force is acceleration dependent. This means that the maximum for each force component occur at different time instants due to the phase difference.

3.4.5 Snap forces

If the accept criteria 3.20 is not fulfilled the upward hydrodynamic forces exceed the static force of the ROV-system, and snap forces in the hoisting line may occur. The snap force is given by:

$$F_{\text{snap}} = v_{\text{snap}} \sqrt{K(M + A_{33})} \tag{3.31}$$

v_{snap} is the snap velocity and K is the stiffness of the system used in the operation. The snap velocity is given by the following equation:

$$v_{\text{snap}} = v_{\text{ff}} + C v_r \tag{3.32}$$

The free fall velocity is given in Equation 3.33 and v_r is given by Equation 3.27 as described earlier.

$$v_{ff} = \sqrt{\frac{2F_{static}}{\rho A_p C_d}} \tag{3.33}$$

C is the correction factor and varies depending on the relationship between v_r and v_{ff}.

$$C = \begin{cases} 1 & \text{for } v_{ff} < 0.2v_r \\ \cos(\pi(\frac{v_{ff}}{v_r} - 0.2)) & \text{for } 0.2v_r < v_{ff} < 0.7v_r \\ 0 & \text{for } v_{ff} > 0.7v_r \end{cases} \tag{3.34}$$

3.5 Hydrodynamic Coefficients

Proper evaluation of the hydrodynamic properties of the structure penetrating the splash zone is an important aspect of determining the wave loading and motion response of the lifted object. The hydrodynamic coefficients depend on the geometry of the structure, Reynolds number and the Keulegan-Carpenter number. In addition, the motion direction, frequency of oscillation and the proximity to the free surface are important parameters. An object's hydrodynamic properties may be estimated theoretically, empirically or by model tests.

3.5.1 Added Mass

The Recommended Practice (DNV-RP) proposes a formulation to calculate the added mass of 3-dimensional bodies. Added mass coefficients for simple 2- and 3-dimensional bodies are listed in the Recommended Practice. Due to the complex geometry of the ROV system, these coefficients cannot be used directly. A common practice is to calculate the added mass of a perforated structure by using the added mass for the non-perforated structure, and taking the effect of the perforation by multiplying by a reduction factor. It is to be noted that these hydrodynamic coefficients are only valid for infinite fluid, far from boundaries like the free surface. Studies performed by Kopsov and Sandvik (1995) and Sandvik et al. (1993) conclude that perforation gives a reduction of the added mass of the object, and an increase of the drag contribution.

Assuming that the ROV is represented by a square prism, shown in Figure 3.2, the C_a may be determined based on the values given for b/a, where a is the length of the cross-sectional side and b is the height. By plotting the given values for b/a and C_a and performing a regression analysis, the appropriate C_a for the square prism in the heave direction is calculated to be 0.78. In addition to this the perforation effect has to be taken into account.

			b/a	C_A
Square prisms	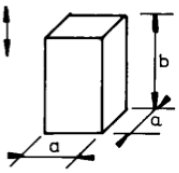	Vertical	1.0	0.68
			2.0	0.36
			3.0	0.24
			4.0	0.19
			5.0	0.15
			6.0	0.13
			7.0	0.11
			10.0	0.08

Figure 3.2: Added mass coefficient of a square prism

Model tests on a Super Scorpio ROV, performed by P. Sayer (Sayer, 2008) concludes that the inertia coefficient C_a (C_m=(1+C_a)) lies in the range 1.4-1.6 for a work class ROV. This means that values of C_a is between 0.4 and 0.6. The same experiment performed on a solid box showed that C_a lies in the range 1.5 - 1.9. As the Super Scorpio is slightly smaller than the Supporter ROV and the solid box less perforated, the inertia coefficient for the ROV is assumed to lie in the

range 1.5-1.8. In another experiment performed by P. Sayer (Sayer, 1996) the hydrodynamic forces on ROVs near the sea surface were investigated. In this experiment it is concluded that the increase of C_a due to the proximity to the free surface has an average of 10% on the Super Scorpio. The inertia coefficient is then adjusted to lie in the range 1.65-1.98, hence the added mass coefficient is in the range 0.65 – 0.98. This is also consistent with the estimation from the Recommended Practice. A conservative estimate of 0.8 is therefore suggested.

3.5.2 Drag

As described in Section 3.3.2 the drag term is expressed by a linear and quadratic drag term for low KC-numbers. B_1 and B_2 in F_R represent the hydrodynamic damping at oscillatory flow. The drag coefficient of oscillatory flow is typically 2-3 times larger than the steady state drag coefficient C_d (Øritsland and Lehn, 1989). The use of a steady state drag coefficient is therefore likely to underestimate the damping and overestimate the resonant motions of the object (DNV, 2011). Nevertheless, the drag coefficient for inertia dominated structures should be chosen with care, as the drag term may induce unrealistic damping to the system (Sarkar and Gumestad, 2010). Experiments show that the linear term has a considerable contribution to the damping and that the KC-dependency is of less importance (Øritsland and Lehn, 1987). By using a linear and quadratic drag term, amplitude dependent coefficients are avoided. The linear and quadratic damping coefficients in Equation 3.14 are expressed as a function of the non-dimensional damping coefficients b_1 and b_2:

$$B_1 = \frac{2\rho A_p \sqrt{2gD}}{3\pi^2} b_1 \tag{3.35}$$

$$B_2 = \frac{1}{2}\rho A_p b_2 \tag{3.36}$$

It may be assumed that the damping energy dissipates through a quadratic term, implying that the B_1 and B_2 are simplified to the drag term of Morison's equation.

$$C_d = \frac{b_1}{KC\omega'} + b2 \tag{3.37}$$

ω' is the non-dimensional frequency of oscillations and D is the characteristic dimension in the flow direction.

$$\omega' = \omega\sqrt{\frac{D}{2g}} \tag{3.38}$$

O. Øritsland has provided a collection of hydrodynamic data for a selection of complex subsea structures (Øritsland, 1989). As there is limited published data of the hydrodynamic properties of the TMS and ROV, this booklet of data has been used to estimate the hydrodynamic coefficients. It is to be noted that the subsea structures in the booklet Øritsland (1989) differ

from the ROV system investigated in this thesis, and the values are therefore critically selected to ensure that the hydrodynamic forces are not underestimated. Added mass and damping for the subsea structures are obtained by decay tests and the drag coefficient in steady flow is determined by towing tests.

The subsea structures described in (Øritsland, 1989) are classified into three categories:

- Buoyant type body - large body with surrounding framework and neutral buoyancy
- Working tool - heavy central part, large mass/buoyancy ratio and added mass of less importance
- Plate shaped structure - large added mass and drag in vertical direction and small in horizontal direction

Based on the fullness factor $\frac{V}{LBH}$ and the weight in air/buoyancy ratio listed in Table 3.2, it is concluded that the properties of the ROV system resemble structure 10, a buoyant structure.

Table 3.2: Comparison of the physical properties of the ROV system and structure 10

Object	Fullness factor	Weight/Buoyancy-ratio
ROV system	0.43	0.38
Structure 10	0.32	0.38

It is seen from Table 3.2 that structure 10 has a smaller fullness factor than the ROV system. This is taken into account when the hydrodynamic properties of the ROV system are decided. The hydrodynamic properties of structure 10 are summarized in table 3.3.

Table 3.3: Hydrodynamic data of structure 10

Motion	C_a	b_1	b_2	C_{ds}
Sway	0.75	0.24	1.89	0.93
Heave	0.75	0.24	1.89	0.93

The fullness factor and the added mass coefficient of structure 10 is slightly smaller than the corresponding values of structure 10. This implies that the non-dimensional damping coefficients should be increased. The coefficients b_1 and b_2 are taken as 0.3 and 1.95. These values may be used in SIMO, which is further addressed in Section 5.4.

As described in Section 4.1 the drag coefficient in OrcaFlex is described as the quadratic drag in Morison's equation. These drag coefficients are determined from model test on the ROV

Dolphin 3K (Nomoto and Hattori, 1986), which has similar main dimensions as the Supporter ROV. The drag coefficients of the Dolphin 3K are presented in Table 3.4.

Table 3.4: Drag coefficient of Dolphin 3K ROV

Surge	Sway	Heave
1.0	1.2	2.0

Experiments performed by P. Sayer (Sayer, 1996) conclude that proximity to the sea surface increases the drag coefficient by 25%. As this is the case for the Supporter ROV the drag coefficients are modified according to the results found by P. Sayer. The drag coefficients of the Supporter ROV are listed in Table 3.5.

Table 3.5: Drag coefficient of Supporter ROV

Surge	Sway	Heave
1.5	2.0	2.5

3.5.3 Water Entry and Exit

Slamming effects occur due to the impact loads between the structure and the water. The slamming coefficient is largest when the object hits the water and reduces with time. (Faltinsen, 1990). According to (DNV, 2011) the slamming coefficient C_s for structures that differ from a smooth circular sylinder should not be taken as less than 5. Due to the limited litterature regarding slamming coefficients on complex structures, it is taken as 5. It is assumed that the ROV plough through the water surface, and the slamming effect may be neglected for the TMS.

For circular cylinders the coefficient may be taken as 3 (DNV, 2011). As the TMS is composed of a number of circular cylinders, the water exit coefficient is assumed to be 3.

3.5.4 Slender Elements

Figure 3.3 shows the high-frequency limit of the vertical added mass coefficient and the corresponding derivative near the free surface. The values are given as a function of submergence h.

At h=-r , where r is the radius of the cylinder, is the time instant when the cylinder interacts with the water surface. The added mass as a function of submergence is shown in Figure 3.3.

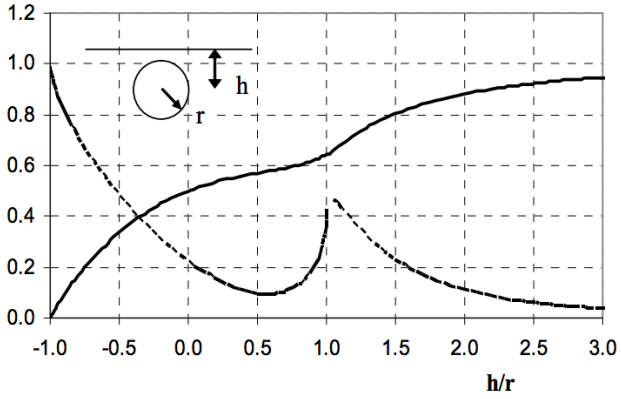

Figure 3.3: High frequency added mass and its derivative near the free surface (DNV, 2010)

The slamming coefficient of a slender element may be expressed as a function of its rate of change of the sectional added mass with submergence h.

$$C_s = \frac{2}{\rho D}\frac{dA_{33}^{\infty}}{dh} \tag{3.39}$$

4 Software Programs

4.1 Theory of OrcaFlex

OrcaFlex is a time domain finite element program commonly used within the offshore industry. The software package is developed by Orcina, and is used for static and dynamic analysis of marine risers, mooring systems, installations and towed systems. The theory described in this section is outlined according to the OrcaFlex User Manual, Orcina (2013).

4.1.1 Analysis

The static analysis is performed in order to determine the equilibrium position of the system used in the dynamic analysis. The dynamic analysis is divided into two steps. It consists of the build-up period, where the waves and the motion of the system are allowed to develop from a still state to a fully developed condition. This is done to reduce the transients that occur in the transformation from the static stage to the fully developed dynamic motion. The build up stage is numbered 0, and the duration of the stage should at least be one wave period. This is to ensure that the motion of the system is fully developed. The second part of the dynamic analysis is the simulation part where the dynamic equation of motion is investigated.

Calculation of the dynamic equation may be performed by explicit or implicit integration. Both integration methods apply the start conditions computed in the static analysis, and solve the new geometry of the system at every time step. This allows OrcaFlex to have control over all geometric nonlinearities, such as the spatial variation of the wave loads. The forces and moments acting on each free body and node in the system are calculated such that the local equation of motion, Equation 4.1, for each object can be established.

$$M\ddot{x} = F - B\dot{x} - Kx \tag{4.1}$$

The solution of the local equation of motion for an object computes the respective acceleration of the object. The explicit integration method uses Euler integration with constant time steps and solves the local equation of motion at the beginning of each time step. The Euler integration method is used implying that the positions and orientations of all nodes and bodies are known at the end of the time step, and the process is repeated. Use of the implicit integration requires an iterative solution for each time step, as the position, velocity and acceleration are unknown at the end of the time step. This causes the implicit method to be more time-consuming than the explicit method. On the other hand, the implicit integration is stable for longer time steps than the explicit integration method and is therefore faster.

4.1.2 Environment

The wave trains in OrcaFlex can be a regular wave, a random wave or specified by a time history. The random waves are generated by a series of sine waves with constant amplitude and pseudo-random phase, that are added together. The phases are chosen using random number generator to assign phases. This means that the same seed will always give the same wave train.

Linear wave theory only defines the wave kinematics up to the mean water level. To predict the wave kinematics above the mean water level OrceFlex offers three types of stretching of the wave kinematics, vertical stretching, wheeler stretching and extrapolation stretching. Vertical stretching replaces the values for z>0 by the values at the mean water level (z=0). Wheeler stretching linearly stretches or compresses the water column into a height equivalent to the mean water depth and the extrapolation method linearly extrapolates the tangent at the mean water level. Without kinematic stretching of the waves, the particle velocity may be predicted to be unrealistically large.

4.1.3 Coordinate systems

OrcaFlex distinguishes between a global and a local coordinate system. The global coordinate system is denoted GXYZ, where G is the global origin and GX, GY and GZ are the axes in the global coordinate system. Each modelled object is denoted with its own local coordinate system, Lxyz. The coordinate systems are right handed with positive rotations clockwise when looking in the direction of the axis in question.

4.1.4 Objects

Vessel

The vessel is free to move in six degrees of freedom, three translations (surge, sway and heave) and three rotations (roll, pitch and yaw). Two types of motions may act on the vessel. These are low frequency motions (LF), like slow drift motion, and wave frequency motions (WF) due to the response from wave loads. These motions may be calculated separately using what OrcaFlex has defined as primary and superimposed motion, where the last motion is superimposed on the first. If the primary motion is set to none, the vessel motion remains fixed at the position calculated in the static analysis. The vessel motions are described by the RAOs, assiged to the vessel's COG.

6D buoy

The 6D-buoy is a rigid body with six degrees of freedom, three translations and three rotations. The hydrodynamic loads on the lumped buoy are calculated using Morison's equation.

$$F_w = (\Delta a_w + C_a \Delta a_r) + (\frac{1}{2}\rho C_d A v_r \mid v_r \mid) \tag{4.2}$$

The first term represents the inertia term, which is dependent of the water particle acceleration. Δ is the mass of the displaced water, a_w is the water particle acceleration relative to the earth, C_a is the added mass coefficient and a_r is the water particle acceleration relative to the body. The second term is the drag force dependent of the water particle velocity. C_d is the drag coefficient for the buoy, A is the drag area and v_r is the water particle velocity relative to the body.

OrcaFlex has tree types of 6D buoys available, lumped buoy, spar buoy and towed fish. The lumped buoy and spar buoy is described further. The lumped buoy is defined without a detailed geometry. Roll and pitch stiffness is therefore not captured by the lumped buoy. This consequently leads to inaccurate results when modelling a buoy penetrating the free surface. When calculating buoyancy for a lumped buoy, the buoy is treated as a vertical stick element with length equal to the specified height of the buoy. The buoyancy changes linearly with the vertical position of the buoy, without taking orientation into account. The hydrodynamic loads for a lumped buoy are calculated at centre of the wetted volume, using fluid kinematics at this position. The loads are scaled by a scaling factor equal to the proportion wet of the buoy, and applied at the centre of wetted volume. To model penetration through the water surface more correct, additional geometric information is needed.

The spar buoy consists of a series of cylinders placed on top of each other, allowing geometrical input for the buoy. The axis of the spar buoy is vertical. The towed fish is similar to the spar buoy, but with a horizontal axis. A spar buoy models the surface piecing effects in a more accurate way as the buoy may be divided into separate cylinders. The buoyancy and hydrodynamic forces are calculated for each separate cylinder defined for the buoy. The loads act in the centre of the wet volume for each cylinder. Buoyancy variation due to the wave is captured because the water surface is assumed to be tangent to the instantaneous wave surface directly above the centre of the cylinder. The heave, roll and pitch stiffness of the buoy are calculated using the intersection of the water surface for each cylinder in the buoy. This allows for immediate position and orientation of each cylinder in the wave.

Since the 6D buoy is able to rotate in 3 degrees of freedom, the buoy requires input values for the rotational forces. Due to the lack of sources regarding hydrodynamic inertia of rotating bodies, OrcaFlex propose to use the moment of inertia of the displaced mass. The hydrodynamic mass

moments of inertia about the x-, y- and z-axis of a rectangular buoy are given below.

$$\begin{aligned} \Delta I_x &= \frac{\Delta}{12}(y^2 + z^2) \\ \Delta I_y &= \frac{\Delta}{12}(x^2 + z^2) \\ \Delta I_z &= \frac{\Delta}{12}(x^2 + y^2) \end{aligned} \tag{4.3}$$

The same problem arises for the moment area used to calculate the drag moment. The drag moment of area is calculated in the following way:

$$\begin{aligned} \mathrm{MA_{dragx}} &= \frac{x}{32}(y^4 C_{\mathrm{dz}} + z^4 C_{\mathrm{dy}}) \\ \mathrm{MA_{dragy}} &= \frac{y}{32}(x^4 C_{\mathrm{dz}} + z^4 C_{\mathrm{dx}}) \\ \mathrm{MA_{dragz}} &= \frac{z}{32}(x^4 C_{\mathrm{dy}} + y^4 C_{\mathrm{dx}}) \end{aligned} \tag{4.4}$$

The slamming force is calculated according to the following equation:

$$F_s = \frac{1}{2}\rho C_s A_w \mid V_n^2 \mid n \tag{4.5}$$

C_s is the slamming coefficient and the slamming area is denoted A_w. This is treated differently for a lumped buoy and a spar buoy. For the lumped buoy the area is given manually, and for a spar buoy it is taken to be the instantaneous water plane area. V_n is the component of the buoy velocity that is normal to the water surface, measured relative to the water particle velocity. The equation also takes the unit vector in the water surface into account. This is to ensure that the slam force opposes the objects penetration of the surface. The slamming force on a lumped buoy is calculated at the centre of the wetted volume. For a spar buoy it is calculated separately for each defined cylinder.

3D buoy

The 3D buoy is free to move in three degrees of freedom, and is restrained from rotation. The properties that may be assigned to a 3D buoy are weight, buoyancy, drag, added mass and reaction forces from other shapes. If the properties of the buoy are neglected, the 3D buoy is well suited for modelling nodes in the system.

Winch

OrcaFlex provides two types of winches, simple and detailed. The simple winch is massless and neglects the winch inertia. It is recommended unless detailed characteristics of the winch drive system are essential in the modelling. The simple winch is connected between two points in the model, and the wire is predefined with a constant tension or a constant speed. The wire is given stiffness and specified length, which is used to calculate the statics of the system. In the dynamic analysis specifying a length, velocity, and acceleration or tension components controls the winch.

Links

The links in OrcaFlex are massless and may be modelled as a tether or a spring-damper system. The tether is an elastic tie that can only take tension, while the spring-damper system can take tension and compression.

4.2 Theory of SIMO

Simulation Workbench for Marine Applications (SIMA) is the graphical interface for the simulation programs Riser System Analysis (RIFLEX) and Simulation of Marine Operations (SIMO). SIMA is a complete tool for simulation of marine operations. RIFLEX is a computer tool for structural and hydrodynamic analysis of slender marine structures and SIMO is used for simulation of motions and station-keeping behaviour of marine systems. As the ROV lift operation investigated in this thesis is simulated in SIMO, this program is further described as outlined in the SIMO Theory Manual (MARINTEK, 2013a).

4.2.1 Equation of Motion

The following equation of motion is solved by SIMO to calculate the load and response history with respect to time.

$$M\ddot{x} + C\dot{x} + B_1\dot{x} + B_2\dot{x} \mid \dot{x} \mid + Kx = q \tag{4.6}$$

M represents the structural mass and the frequency dependent added mass matrix, C is the frequency dependent potential damping matrix, B_1 and B_2 is the linear and quadratic damping matrix and K is the hydrostatic stiffness matrix. Position, velocity and acceleration is denoted x, $\dot{x}$ and $\ddot{x}$ respectively. The excitation vector is expressed as q.

The equation of motion may be solved by convolution integral or by separation of motion. The first method, solution by convolution integral, solves the whole differential equation in the time domain by the use of retardation function. This is only used if a frequency-dependent added mass and damping is modelled. The second method separates the motions into a high frequency (HF) and a low-frequency (LF) term. The HF motions are solved in the frequency domain. This is based on the assumption of linear response of the structure when it is subjected to incoming waves. The LF motions are solved in the time domain.

4.2.2 Coordinate Systems

SIMO makes use of four different right-handed Cartesian coordinate systems. The global coordinate system is earth-fixed, and is referred to by the local body coordinate system. The local body coordinate system is body-fixed and therefore follows the movement of the body. The body-related coordinate system follows the body's horizontal motion. This coordinate system is referred to by forces and motion transfer functions. The last coordinate system is the initial coordinate system. When the simulations begin, this system coincides with the body-related system and is fixed throughout the simulation.

4.2.3 Environment

Linear wave potential theory is used to describe a regular wave in SIMO. Irregular waves are modelled as a sum of regular waves with different frequencies. An irregular wave spectra may be described by the JONSWAP and PM-spectrum as outlined in Section 3.2.

4.2.4 Bodies

SIMO offers three types of bodies in addition to a predefined body type.

1. Large volume body with 6 DOF, the total motion is calculated in the time domain
2. Large volume body with 6 DOF, the motion is separated into a frequency domain (HF motions) and a time domain (LF motions)
3. Small volume body with 3 DOF

For vessel motion described by the first order transfer functions (RAO), the body motions are separated into a frequency domain and a time domain as described earlier. The RAOs are solved in the frequency domain. In addition to the transfer functions a hydrostatic stiffness for heave, sway and yaw needs to be defined for the vessel. These values may be obtained using the water plane area A_{wp} and the transverse and longitudinal metacentric heights GM_T and GM_L through the following relations:

$$k_{33} = \rho g A_{\text{wp}} \tag{4.7}$$

$$k_{44} = MgGM_T \tag{4.8}$$

$$k_{55} = \rho g MGM_L \tag{4.9}$$

To control the position of the vessel in SIMO, a simplified dynamic positioning (DP) system may be modelled by using horizontal springs or values for surge, sway and yaw in the stiffness and damping matrix. Damping due to a DP-system may be taken as 70% of the critical damping, B_{crit}.

$$B_{\text{crit}} = 2\sqrt{kM} \tag{4.10}$$

4.2.5 Distributed Element

Two types of distributed elements are available in SIMO. These are slender elements and fixed body element with no extension. Slender elements may be used as substructures when modelling larger structures as jacket legs or subsea structures. The slender elements are divided into strips, where the force contributions are calculated for each strip and then summarized. The force contributions are gravity and buoyancy forces, slamming forces and wave forces. A stiff connection implies that the slender element forces are calculated and

transferred to the defined main body.

The wave forces are calculated by Morison's equation with an additional linear term. The force in a single strip is taken as:

$$F_{\text{slender}} = (\rho V + \rho V C_a) a_w + B_2 v_r |v_r| + B_1 v_r \tag{4.11}$$

The first term represents the Froude-Krylov and diffraction force proportional to the water particle acceleration. The second term is the quadratic drag dependent of the square relative velocity and the last term is the linear drag. V is the submerged volume per length unit.

The distributed elements may be defined with depth dependent coefficients. As seen in Figure 3.3 in Section 3.5.4 the added mass varies with the proximity to the free surface. If the object is fully submerged, these coefficients are not of interest. The depth dependent coefficients are defined at the centre of each strip and are used for horizontal elements. For tilted elements a scaling factor is calculated, which is proportional to the submerged part of each strip (MARINTEK, 2013b).

The slamming force acting on a slender element is related to the change in added mass, as the object is lowered through the wave zone. This is seen from Equation 3.14. However, when a slender element with nearly horizontal angle crosses the water surface, the slamming force is calculated only if the position dependent data are given. It is to be noted that slender elements do not recognize each other, and therfore they do not cause any interaction between each other.

4.2.6 Body Components

The bodies defined in SIMO are allowed to be defined with a body point relative to the body-related coordinate system. The body points may be modelled with a winch system. The winch is defined with wire paid out, wire length left on the drum and maximum acceleration and speed. Four different types of coupling elements may be defined to the winch, simple wire coupling, multiple wire coupling, fixed elongation coupling or a user defined coupling. The simple wire coupling is modelled as a linear spring according to Hook's law:

$$\Delta l = \frac{F}{K} \tag{4.12}$$

The effective axial stiffness is given by

$$\frac{1}{K} = \frac{l}{EA} + \frac{1}{k_0} \tag{4.13}$$

The first term represents the axial stiffness and the second term is the flexibility of the crane. The flexibility stiffness takes the flexibility of the crane and the elasticity of the wire into account. The material damping in the line may be taken as 1-2% of EA (MARINTEK, 2013b).

5 Methodology

5.1 Analytical Calculations

DeepOcean utilizse a standardized spreadsheet developed within the company to perform analytical calculations according to the Simplified Method. This spreadsheet has been used as a basis for the analytical calculations presented in this section. The heave response of the LARS crane tip is established by importing RAO-data for Edda Flora (Lien, 2009) into OrcaFlex. Further, OrcaFlex computes the ship response in an irregular sea state, described by the JONSWAP-spectrum, and calculates the heave response at the position of the LARS crane tip position. The heave response of the crane tip is described by an amplitude, velocity and acceleration for T_z varying from 1-13 s and H_s varying from 0.25-7 m with intervals of 0.25 m. These values are implemented in the spreadsheet used for the analytical calculations.

5.1.1 Environment

As described in Section 3.2, the analyses should be performed at least ±15 ° off vessel heading. For simplifications, only the waves approaching the vessel 15° off vessel heading are considered in the analytical calculations. This is implemented in the analytical calculations through the RAOs exported from OrcaFlex. According to equation 3.7 the lower T_z value is determined by the H_s used in the analysis. The analysed H_s and the corresponding T_z range is presented in table 5.1. Wind and current are neglected in the analyses.

Table 5.1: Environmental parameter variation

H_s [m]	T_z [s]	ζ_a [m]
2.5	5-13	2.25
3.0	5-13	2.70
3.5	6-13	3.15
4.0	6-13	3.60
4.5	7-13	4.05
5.0	7-13	4.50

5.1.2 ROV Model

The perforation ratio for the ROV is assumed to be 10% of the solid box the main dimensions of the ROV make up. The perforation ratio is used for calculating the heave projected area of object. The TMS is more perforated than the ROV, and the perforation ratio is taken as 20%. This has been estimated from drawings of the system provided by DeepOcean enclosed in Appendix A.1. The hydrodynamic properties of the TMS and ROV are summarized in table 5.2.

Table 5.2: Hydrodynamic property of the ROV and TMS

Hydrodynamic property	ROV	TMS
C_a	0.8	0.8
C_d	2.5	2.5
C_s	5	0

5.1.3 Load Cases

As the ROV and TMS are being lowered through the splash zone, there will be different hydrodynamic loads acting on the system at different stages of the operation. The analyses performed in the Simplified Method are stationary analyses, where the relevant properties are taken into account for each analysis. Four different load cases have therefore been defined.

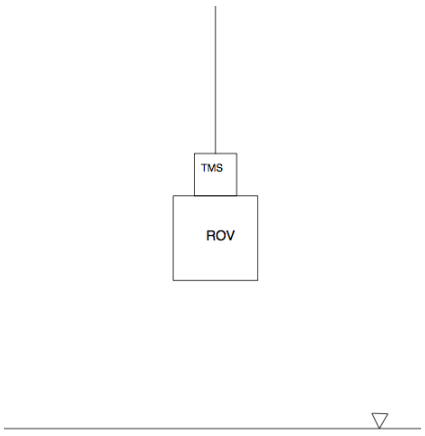

Figure 5.1: Load case 1

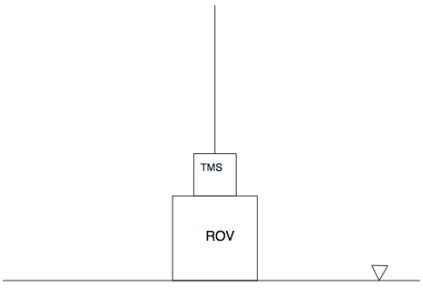

Figure 5.2: Load case 2

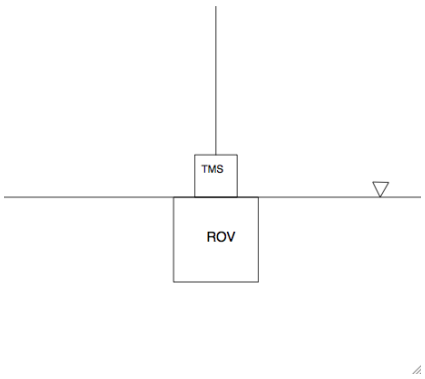

Figure 5.3: Load case 3

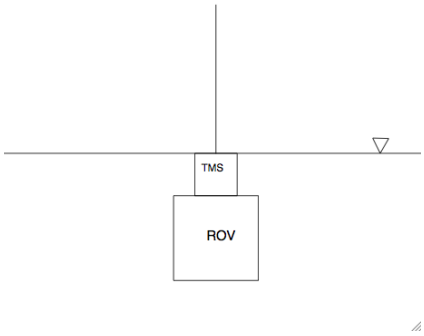

Figure 5.4: Load case 4

Load case 1 - ROV and TMS hanging in the air

For load case 1 the ROV system is hanging in the air, and does not interact with the water. The motion of the ROV system is only dependent of the vessel motions.

Load case 2 - TMS and ROV above the sea surface

In load case 2 the ROV and TMS are hanging right above the sea surface. An impact slamming force will act on the bottom of the ROV. A varying buoyancy force due to the wave elevation will also act on the structure. The slamming force will be at its largest where the vertical water particle velocity v_s is at its maximum. From Figure 3.1 it is seen that this occurs at the mean water level. To obtain a worst-case scenario the lowest part of the ROV system is therefore assumed to hold this position.

Load case 3 - ROV fully submerged, TMS above the sea surface

In load case 3 the ROV is fully submerged, while the TMS is still above the sea surface. The forces acting on the ROV will be the varying buoyancy force, the mass force and the drag force. The vertical water particle velocity and acceleration are related to the distance from the free surface to the vertical COG of the ROV. The TMS will experience some varying buoyancy force due to the wave elevation. Added mass caused by the wave elevation is assumed to be zero, and the mass force of the TMS is therefore only influenced by the heave acceleration of the crane tip. The slamming forces in the TMS are neglected, as it is assumed that the ROV makes a shadowing effect for the TMS as the system penetrates the water.

Load case 4 - TMS and ROV fully submerged

For the last load case the TMS and ROV are fully submerged, and the still water level is above the ROV system. The slamming force and varying buoyancy force is zero for this case. The mass force is calculated separately for the TMS and ROV, using the vertical water particle acceleration for the corresponding COG. The total mass force is the sum of the two contributions, as described in Equation 3.24. The total drag force is calculated in the same way using the vertical water particle velocity for the corresponding COG of each of the structures.

5.1.4 Snap Forces

If the acceptance criteria, Equation 3.20, is not fulfilled, a further investigation of the snap forces in the hoisting line has to be performed. The snap forces are calculated according to equation 3.31. The length of the wire is modified to represent each load case. For load case 2 the snap velocity is assumed to equal v_s, since v_{ff} becomes zero for this load case. For load case 3 v_r is used relative to the submerged ROV, and for load case 4 v_r is used relative to the submerged TMS. The correction factor C is 1 for both of the latter load cases.

5.2 Time Domain Analyses

The large non-linearities that occur during lowering through the splash zone are best taken into account by simulating the operation in a time domain computer program. This is more accurate than the analytical calculations outlined by the Simplified Method described in Section 3.4. The time domain analysis numerically integrates the equation of motion described in Section 3.3.

Simulations in an irregular sea are normally performed a large number of times to achieve statistical confidence. An alternative approach is to investigate the maximum relative velocity or acceleration between the crane tip and the vertical component of the wave elevation. This approach to the find the limiting sea state is not intended for timing of the launching operation, only as an alternative to repetitive simulations for statistical confidence. Whether it is the maximum relative velocity or the maximum relative acceleration that represents a worst-case scenario, is investigated in Section 6.2.

5.3 Modelling in OrcaFlex

The following section describes the modelling of the vessel, lifting system and the ROV-system in OrcaFlex. The simplifications of the modelling are also presented.

5.3.1 Vessel and Launching System

The vessel origin is defined to be positioned at AP at the keel. The position of the vessel origin is manually defined. The RAOs describing the first order motions of the vessel is defined at the vessel's COG as listed in Table 2.1.

The stiffness of the launching crane is taken into account by modelling a link as a tether. The stiffness of the link is given by the stiffness of the LARS. One end of the link is positioned relative to the vessel, and the other end is connected to a 3D buoy. The 3D buoy is modelled with negligible properties, and represents the crane tip in the model. Giving 3D buoys negligible properties is a useful modelling technique for modelling nodes in the system. The 3D buoys may be connected to other objects in OrcaFlex such as a winch. The winch represents the launching wire in the model, and is given the stiffness properties of the umbilical. In the simulations the winch is driven up over a period of 3 s to avoid transient effects due to rapid changes in the simulations. Before the ROV system crosses the wave zone the velocity of the pay-out rate is equal to the hook lowering velocity of 0.5 m/s.

5.3.2 ROV Model

Two models of the ROV system have been investigated. The first model, herby named ROV model 1, was established in the project thesis. ROV model 1 is modelled as a single lumped buoy with the geometry of an equivalent, rectangular box. The lumped buoy is given its own local reference frame Bxzy, allowing centre of mass and centre of volume to be specified relative to this. The buoy is given a vertical dimension height, which is assumed to have the midpoint at the centre of volume. The COG and centre of buoyancy (COB) is adjusted to represent the properties of the TMS and the ROV. The hydrodynamic properties of the lumped buoy are given by Equations 4.3 and 4.4.

Six lumped buoys and one spar buoy model the second ROV model, herby named ROV model 2. The spar buoy represents the TMS due to the cylinder-shaped geometry. The ROV is divided into two separate lumped buoys. The last four lumped buoys are modelled as slamming buoys, where only the slamming components are given as input. The total slamming area is the same as for ROV model 1, but it is distributed between four lumped buoys. The four lumped buoys allow the slamming loads to be calculated more accurately than for the ROV model modelled only with one lumped buoy. If the waves interact with one slam buoy, but not the other three, this is captured when distributing the slamming components between the buoys. The hydrodynamic properties of the ROV system is given in Table 5.3. A total summary of the input used for the two ROVs is given in Appendix A.2.

Table 5.3: Hydrodynamic coefficients of the ROV-system

Hydrodynamic property	x	y	z
C_a	0.8	0.8	0.8
C_d	1.1	1.5	2.5
C_s			5
C_e			3

5.3.3 Analyses

In accordance with the recommendations from Orcina (Colin Bludell) the implicit method is used for solving the equation of motion and the vertical stretching of the wave kinematics is applied for the waves. The time step used in the dynamic analyses is 0.01 s. The simulations are dived up into four stages. Stage 0, the build up stage is set to 13 s, which is at least one wave period. Stage 1 represents the simulation time before the maximum relative velocity occurs, in stage 2 the acceleration of the winch is activated and in stage 3 the lowering speed is adjusted to 0.5 m/s, and the penetration through the wave zone take place.

As described in section 3.4.1 the analysis has to be performed 15° off vessel heading if the operation is to be performed independent of the vessel heading. The sea states of interest is limited by Equation 3.7. Each sea state is investigated for head sea and ± 15° off vessel heading. This results in a total of 144 sea states.

Firstly the Python Scripc 'PreProRelativeVelocity.py' generates each sea state by systematically varying the environmental conditions with OrcaFlex commands. An OrcaFlex base data file with duration of three hours is included as base file. Through the OrcaFlex batch-processing task, the 144 text files are simulated in one run, only changing the environmental values in the base file. The batch processing may be done as an overnight job, allowing for large amounts of simulations in an unattended mode.

Further, the maximum relative velocity between the crane tip and the vertical component of the sea velocity is investigated in the Python script 'PostProRelativeVelocity.py' in Appendix E.1. Python communicates with OrcaFlex through the external programming interface OrcFxAPI. The maximum relative velocity and the corresponding time instant for each of the 144 cases is written to an Excel spread sheet.

A new set of text files are generated in the Python script 'PreProRunSimulation.py' in Appendix E.2. This script derives the time instant for the maximum relative velocity for each sea state from the spreadsheet described above. The winch is set to be activated a given time before the maximum relative velocity occur such that the time of impact with the water, is the time instant of maximum relative velocity. As time to impact from the winch is activated varies for each sea state, the winch activation time before the time instant of maximum relative velocity, is varied. At last, the winch tension is investigated in the script 'PostProLiftLineTension.py' in Appendix E.3. These values are written to a new spread sheet, where the minimum tension for each sea state is investigated.

5.4 Modelling in SIMO

The following section presents the modelling of the vessel, lifting system and the ROV model established in SIMO.

5.4.1 Vessel and Launching System

As described in Section 4.2 the vessel is modelled as body type two where the motions are separated into frequency domain and a time domain. The linear response of the vessel is described by the pregenerated RAO functions. As the vessel in SIMO prefers diffraction program like WADAM or WAMIT, the RAO data are defined for a support vessel in RIFLEX and copied to the ship defined in the SIMO task. The values for hydrostatic stiffness are given by the Equations 4.7 - 4.9 as described in 4.2.

To avoid drift off of the vessel when the ROV system is included in the simulation, a simplified dynamic positioning (DP) system has been modelled according to the recommendations from SIMO user manual (MARINTEK, 2013a). As addressed in Section 4.2 the DP system may either be modelled with horizontal springs as a moored vessel, or with realistic values for the stiffness and damping in surge, sway and yaw. The damping due to a DP system is assumed to be 70% of the critical damping, B_{crit}. These values are unknown for the vessel, therefore a preliminary study of the vessel motions has been performed in the last section of this chapter to ensure that the main motions affecting the crane tip movement resemble the motions of the vessel in OrcaFlex.

The crane tip is defined as a body point relative to the vessel's origin in SIMO. Body points in SIMO allows for modelling of winches. The winch speed is driven up over time to reduce transient effects due to the start up of the simulation. A simple wire coupling is connected to the winch in one end, and to the top of the TMS in the other end. The simple wire coupling is modelled with a flexibility stiffness representing the stiffness of the crane, a material damping and axial stiffness.

5.4.2 ROV system

The ROV system is modelled as body type one with six degrees of freedom. The motions of the ROV system are calculated in the time domain. The SIMO theory manual advises to model subsea structures by dividing the structure up into simple structural elements represented by slender element in SIMO. Each slender element contributes to the total mass, buoyancy, added mass and drag of the structure. The TMS is composed of 24 slender elements, while ROV consists of 20 different elements. The model may be seen in Figure 5.5. The properties of the slender

elements are adjusted and tuned to resemble the properties of the ROV system in the best possible way. As described in Section 4.2, the slender elements are allowed to be denoted with depth dependent coefficients. Values from Figure 3.3 used for the slender elements are given in Table 5.4. The depth dependent coefficients for drag is assumed to equal the ratio of the relative submerged volume as there have been found no literature regarding this.

Table 5.4: Depth dependent added mass

$\frac{h}{r}$	$\frac{m_a}{\rho\pi r}$	V_r
-1.00	0.00	0.00
-0.50	0.50	0.19
0.00	0.50	0.50
0.50	0.55	1.81
1.00	0.65	1.00
1.50	0.80	1.00
2.00	0.89	1.00
2.50	0.96	1.00
3.00	0.98	1.00

The longitudinal axis of the slender elements is the local x-axis, and the axes in the y- and z-direction represent sway and heave. The values for the hydrodynamic properties for the x-axis are therefore not defined. The added mass is given for the cross section of the strip section defined for the slender element. In the case where Morison's drag is used, the quadratic drag is modelled as seen in Equation 5.1. The drag is also modelled with a linear and quadratic term as given in Equations 3.35 and 3.36. B_1 and B_2 are proportional to the relative velocity and the quadratic relative velocity. The coefficients are defined per strip, with the diameter of the slender element taken as the projected area of the strip. Equations 5.3 and 5.3 are rearranged to represent the drag of a strip of the slender elements. A total summary of the input data for the ROV system may be found in Appendix A.2.

$$\frac{F_D}{v_r \mid v_r \mid} = \frac{1}{2}\rho D C_d \tag{5.1}$$

$$\frac{F_{B_1}}{v_r} = \frac{2\rho D\sqrt{2gD}}{3\pi^2} b_1 \tag{5.2}$$

$$\frac{F_{B_2}}{v_r \mid v_r \mid} = \frac{1}{2}\rho D b_2 \tag{5.3}$$

The slamming effect is taken into account for the slender elements with defined depth dependent coefficients. The slamming on the vertical elements of the model is neglected as

this area is negligible compared to the rest of the ROV system.

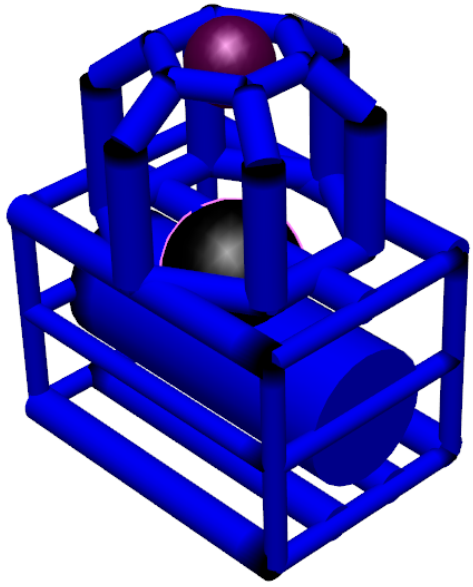

Figure 5.5: ROV model in SIMO

5.4.3 Vertical Velocity

To extract values of the vertical water particle velocity a distributed element is modelled as a dummy node. No forces are set to act on this element; it only follows the sea elevation at the point where the ROV system will interact with the water.

5.4.4 Dynamic Analyses

For splash zone analyses in SIMO the following setting should be used:

- The force should be integrated to the wave surface
- The gravity force and buoyancy should be included
- The wave particle velocity and acceleration should be included

The time step used in the analyses performed in SIMO was set to 0.1 s, with 10 subdivisions per time step to improve the accuracy of the results. The subdivisions are not stored in the time series generated in the analyses. Unlike OrcaFlex, SIMO does not have a build up period allowing transient effects to settle. By ensuring that the lowering operation is performed a sufficient time into the simulation, the transient effects are avoided in the results.

5.4.5 Post Processing

SIMA's built in post processor task is used to analyse the results from the lifting simulations. The relative velocity between the crane tip and the water surface is found by transforming the vertical position of the ship to the position of the crane tip. This time sequence is differentiated to find the vertical velocity of the crane tip. The water elevation at the distributed element is also differentiated such that the vertical velocity is obtained. The absolute value of the relative velocity between the two components is then exported to a data file. The sequence of this is illustrated in Figure 5.6. The results from SIMO are investigated and plotted in MATLAB.

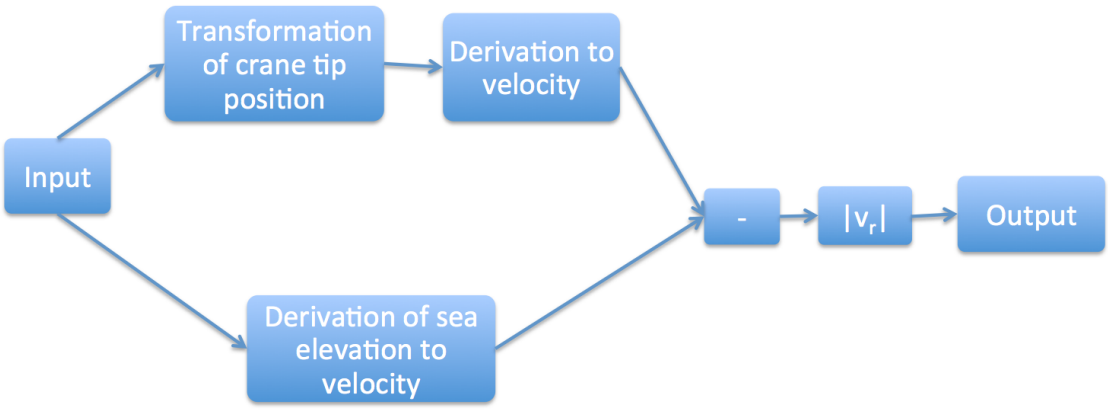

Figure 5.6: Post processing in SIMA

5.5 Modelling Validation

A preliminary study of the vessel motions has been performed in order to validate the modelling of the vessel motions. It is also performed to detect differences in the way the two software programs handle their input data. The simulations are performed in regular waves with ζ_a = 2 m, T = 11 s and head sea. The RAO data are input for both vessels.

The OrcaFlex vessel is simulated with the ROV system hanging from the crane tip, while the SIMO vessel is simulated without the ROV vessel and no additional DP system. Hydrostatic stiffness values are given as described in Section 4.2. Figures 5.7 - 5.9 illustrate the vessel motions for the two vessles in surge, heave and pitch. It is to be noted that the vessel origin for OrcaFlex is at the stern and keel, and the vessel motions are therefore transformed to the COG where the RAOs are given.

According to the official RAOs given by Lien (2009) the motion amplitude in surge for the vessel in waves with ζ_a = 2 m and T = 11 s is 1.44 m. In heave the amplitude is 1.5 m and in pitch 3.44°. The overall trend is that OrcaFlex gives accurate results, while SIMO overestimates the vessel motions. The small deviation in the oscillation amplitude for heave and pitch is believed to origin from the stiffness matrix values that need to be defined for the SIMO vessel. In OrcaFlex the motions from the RAOs are superimposed on a fixed position, while SIMO requires an additional hydrostatic stiffness matrix to avoid capsizing. Sway, roll, and yaw are zero for both vessels.

When the ROV system is attached to the crane tip of the SIMO vessel, the vessel experiences additional motions in roll, sway and yaw. It is observed that these motions originate from LF motions and influence the global motions in the six degrees of freedom. These motions are minimal due to the relatively light weight of the ROV. The LF induced motions would have been considerably larger with a heavier object hanging from the crane. The motions are controlled by a simplified DP system as described in Section 4.2. Due to limited data for critical damping and stiffness values for the vessel, these values are chosen in an iterative process such that they resemble the motions of a vessel with a DP system. The total vessel motions from are plotted in Appendix D.

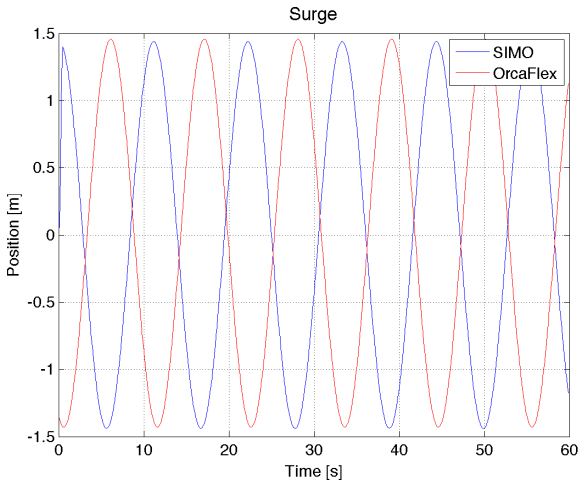

Figure 5.7: Surge motion

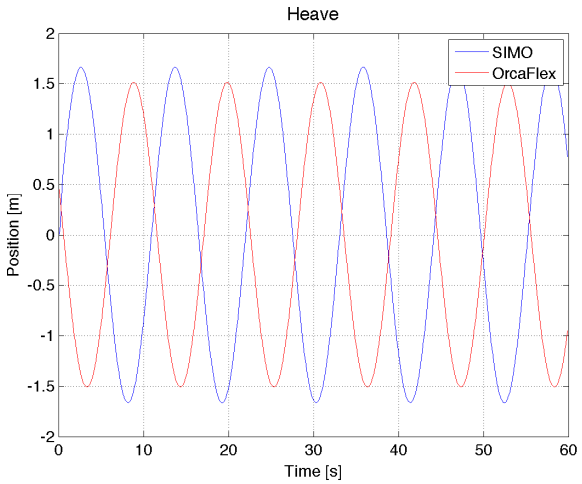

Figure 5.8: Heave motion

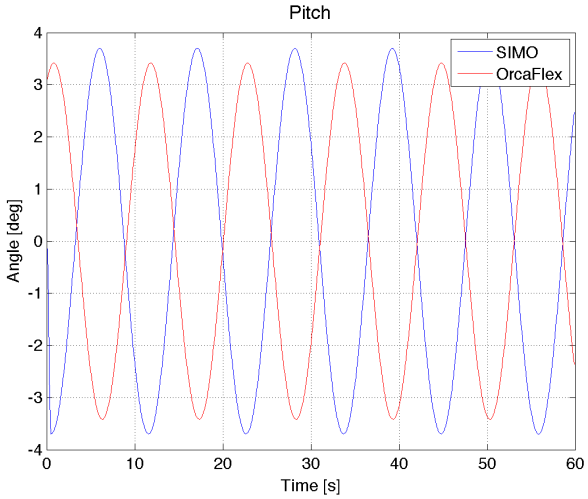

Figure 5.9: Pitch motion

As an additional validation, the vertical motion of the two modelled crane tips are investigated. The same environment as described above is used. Figure 5.10 shows the crane tip position for the vessel modelled in SIMO and OrcaFlex. It is to be noted that the crane tip position in OrcaFlex is represented by a 3D buoy connected to a link. In SIMO, the crane tip position is transformed relative to the vessel's position of COG, and therefore follows the motion of the COG. These differences induce a small deviation of the two crane tip positions.

Figure 5.11 illustrates the difference in the lift line tension for SIMO and OrcaFlex when the ROV system is hanging in the air. The difference between the two cases origin from the flexibility stiffness of the crane, which needs to be modelled in SIMO. In OrcaFlex this is taken into account by a link modelled as a spring, connected to the crane tip 3D buoy.

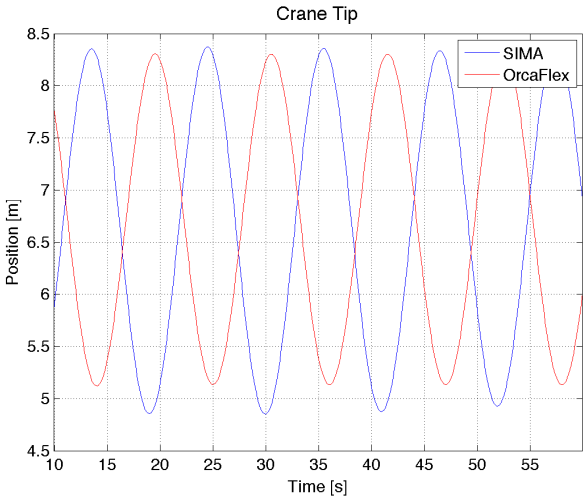

Figure 5.10: Crane tip position

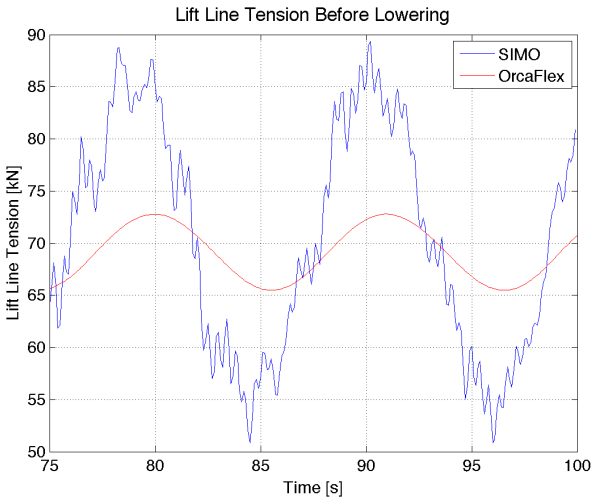

Figure 5.11: Lift line tension for ROV-system in air

6 Results

6.1 Analytical Calculations

This section presents the results from the analytical calculations performed according to the Simplified Method described in Section 3.4. In Table 6.1 the static force for each load case is presented and Figures 6.1 and 6.2 show how the velocity and acceleration of the crane tip vary with different T_z values.

Table 6.1: Static force of the ROV system in each loadcase

	F_{static}[kN]
Load case 1	69.2
Load case 2	69.2
Load case 3	39.2
Load case 4	26.5

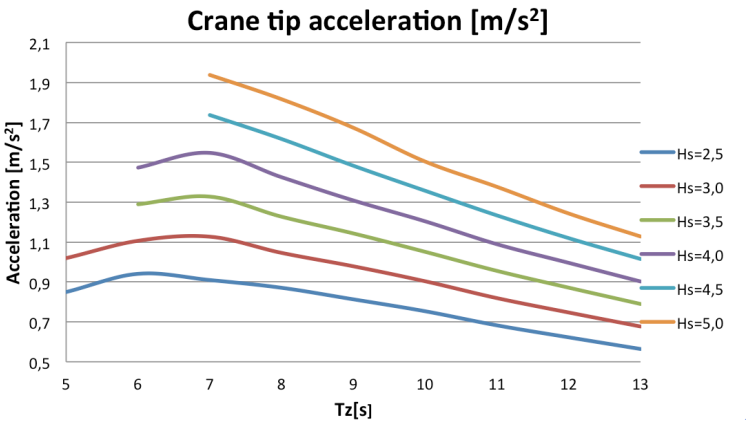

Figure 6.1: Acceleration of crane tip

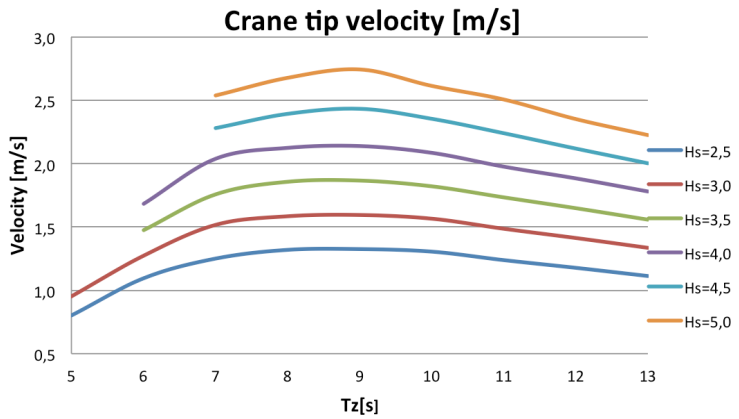

Figure 6.2: Velocity of crane tip

The four following figures present the hydrodynamic force and the corresponding accept criteria, Equation 3.20, for each load case. H_s values 2.5-5.0 m are included while results from the lower H_s values may be found in Appendix C.1. Load case 1 is within the defined accept criteria, while the hydrodynamic forces for load case 2, 3 and 4 exceed the accept criteria. The magnitude of the snap forces that are likely to occur in load case 2, 3 and 4 are included in Appendix C.2. The hydrodynamic forces and the potential snap loads are discussed in Section 7.1.

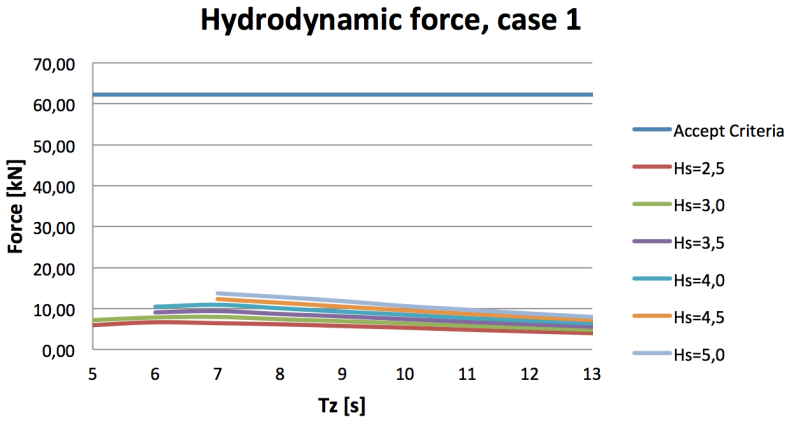

Figure 6.3: Hydrodynamic force for load case 1

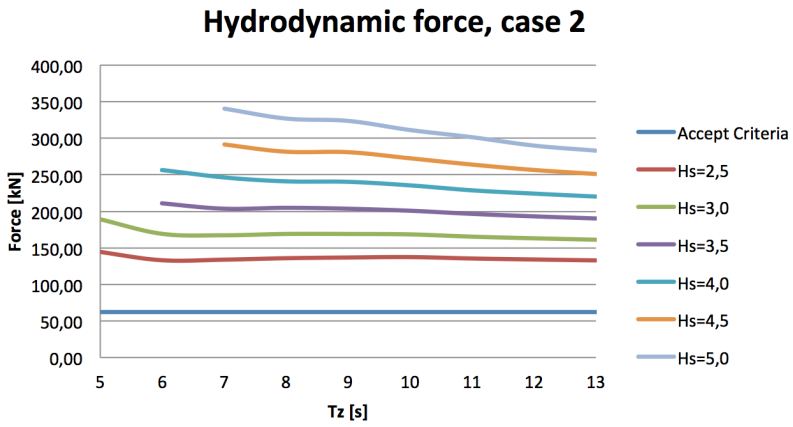

Figure 6.4: Hydrodynamic force for load case 2

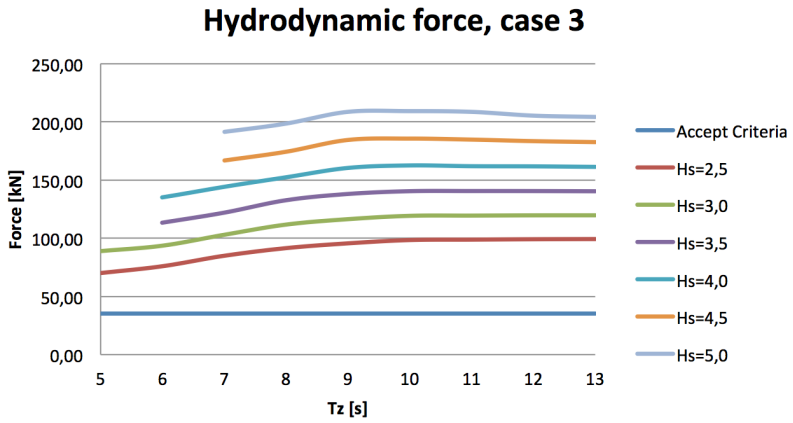

Figure 6.5: Hydrodynamic force for load case 3

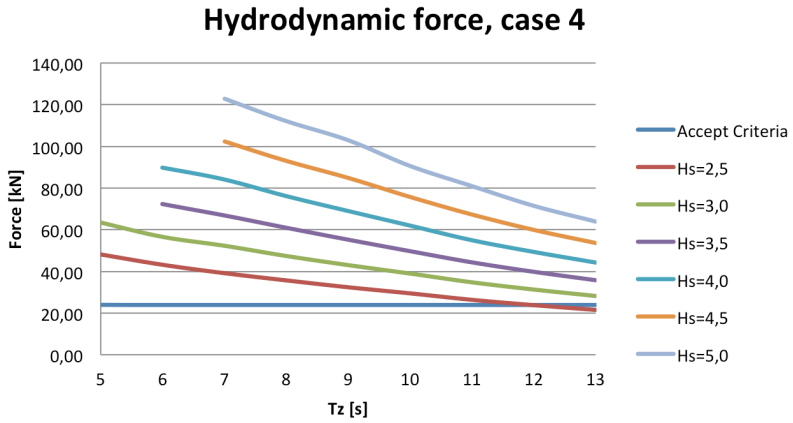

Figure 6.6: Hydrodynamic force for load case 4

6.2 Worst Case

As described in Section 5.2 the time domain simulations may either be investigated a large number of times to obtain a statistical confidence, or at a worst case condition. The relative velocity and the relative acceleration between the vertical component of the crane tip and the vertical component of the waves are investigated to form a basis for the analyses performed based on the relative motion. The study is performed in OrcaFlex, but assumed to form a basis for the analyses performed in SIMO as well.

A three hour sea state with H_s = 4.5 m, T_z = 11 s and head sea is used in this study. 15 different seeds are investigated, where the sea state with the largest relative velocity or acceleration is used further in the analysis. The maximum relative velocity of 1.44 m/s is found in sea state 15 and the maximum relative acceleration of 2.12 m/s^2 is found in sea state two. The ROV system is lowered such that the time instant of maximum relative velocity or maximum relative acceleration corresponds to when the ROV hits the water. The lift line tension for the two cases are plotted in Figure 6.7 for comparison. The case based on impact with the water at the time instant of maximum relative velocity shows a significant reduction in the lift line tension compared to the case where the impact takes place at the time instant of maximum relative acceleration.

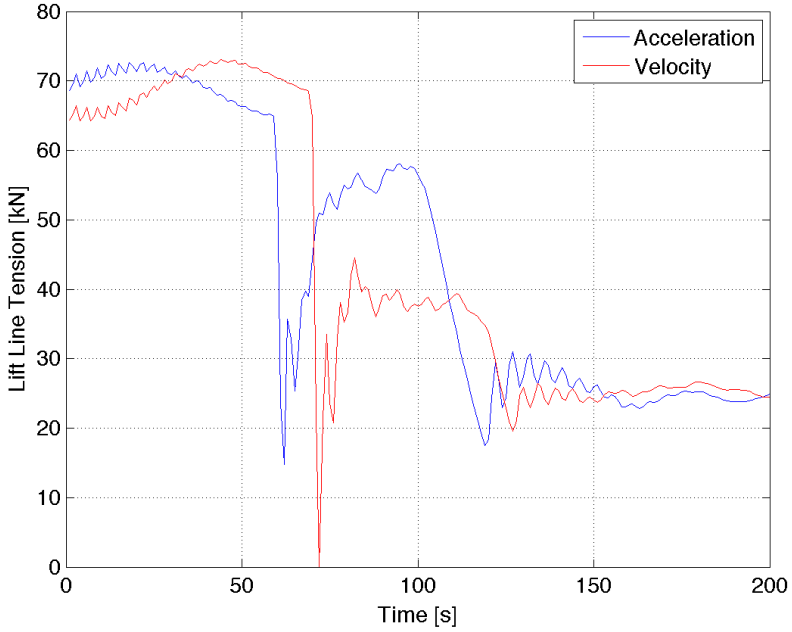

Figure 6.7: ROV-system lowered at the time instant of maximum relative velocity and acceleration

As a validation of the approach of using the maximum relative velocity as a worst-case scenario, 20 simulations at random time instants have been performed. The simulations are carried out in sea state 15, which contained the largest relative velocity between the crane tip and the sea elevation out of the 15 investigated seeds. The lift line tension is above 9.5 kN for all of the lowering simulations performed at random time instants.

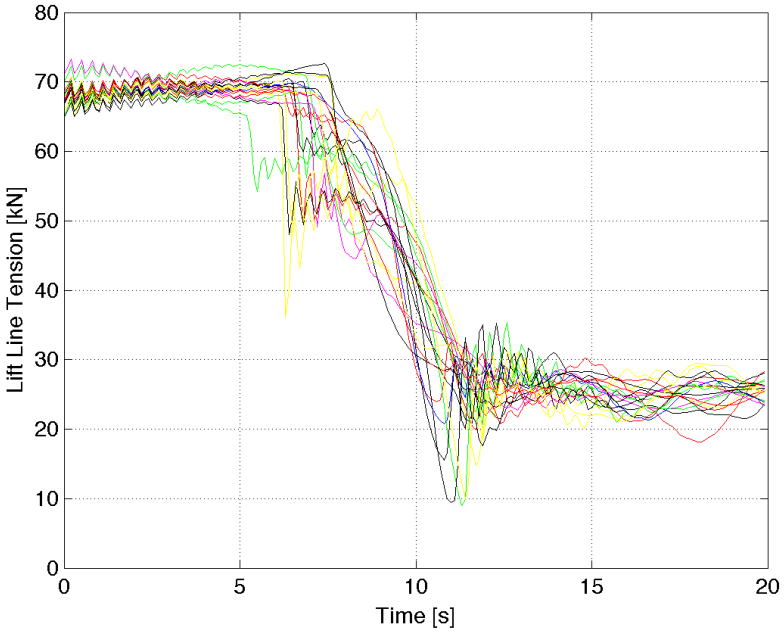

Figure 6.8: ROV-system lowered at random time instants

6.3 OrcaFlex

As outlined in Section 5.3 two ROV models have been investigated in OrcaFlex. ROV model 1 is a simple lumped buoy and ROV model 2 is a more detailed model with a total of six lumped buoys and one spar buoy. Figure 6.9 illustrates the difference in lift line tension with ROV model 1 and 2. It is to be noted that ROV model 2 hits the water at an earlier time instant, and therefore the lift line tension is reduced at an earlier stage.

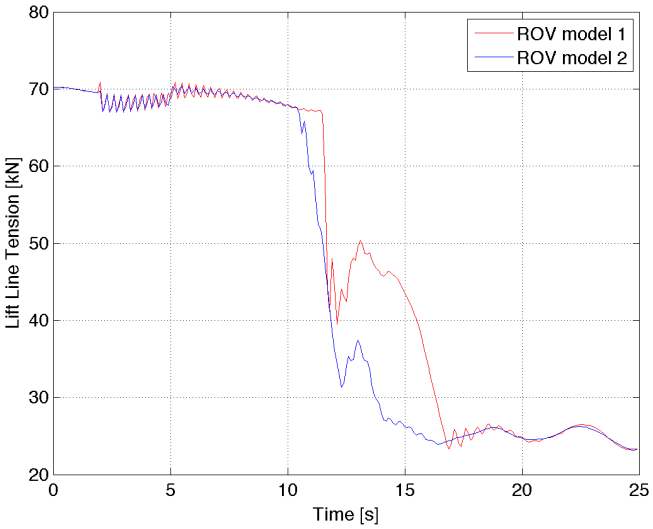

Figure 6.9: Lift line tension for ROV model 1 and 2

6.3.1 Parameter Variation

A study of the hydrodynamic coefficients has been performed in order to determine uncertainties of the estimated hydrodynamic coefficients described in Section 3.5, and the importance of them during penetration of the wave zone. The hydrodynamic coefficients used in OrcaFlex are investigated in a sea state with head sea, H_s = 4.5 m and T_z = 11 s. The simulations are started at the same time instant, implying that the wave profiles are the same in every simulation. The lift line tension in each parametrical study is compared to a base case where the coefficients are as listed in Table 6.2. The base case settings are same for ROV model 1 and 2. The basis for the variation has been discussed in Section 3.5.

Table 6.2: Base case settings

	x	y	z
C_a	0.8	0.8	0.8
C_d	2.0	1.5	2.5
C_s	-	-	5

Added mass coefficient

As discussed in Section 3.5.1 C_a lies in the range of 0.65 - 0.98. A study of the magnitudes of C_a has been performed. Figure 6.10 and 6.11 illustrate the lift line tension of ROV 1 and 2 in the time interval of penetration through the water surface. The plots show the base case described previously and added mass coefficients for the lower and upper values in the C_a-range.

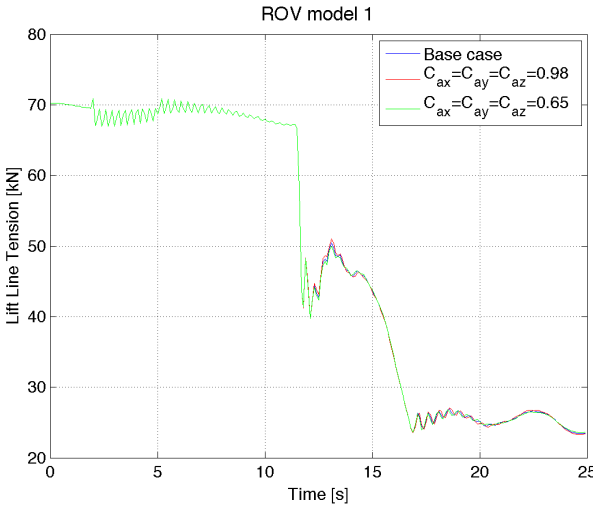

Figure 6.10: ROV 1 - Base case and C_a-range

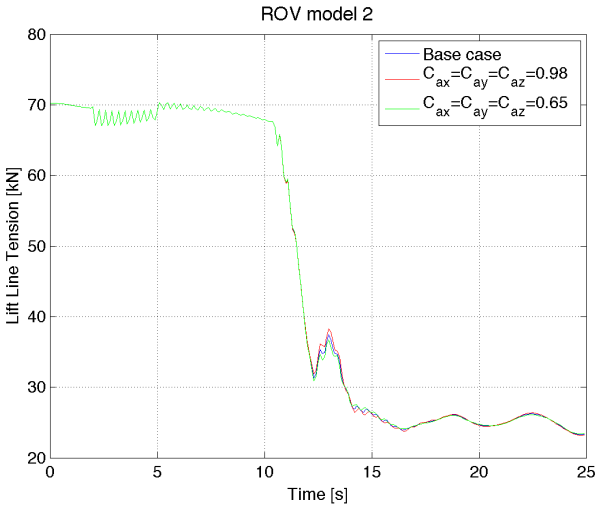

Figure 6.11: ROV 2 - Base case and C_a-range

In Figure 6.12 and 6.13 the added mass is neglected for ROV 1 and 2.

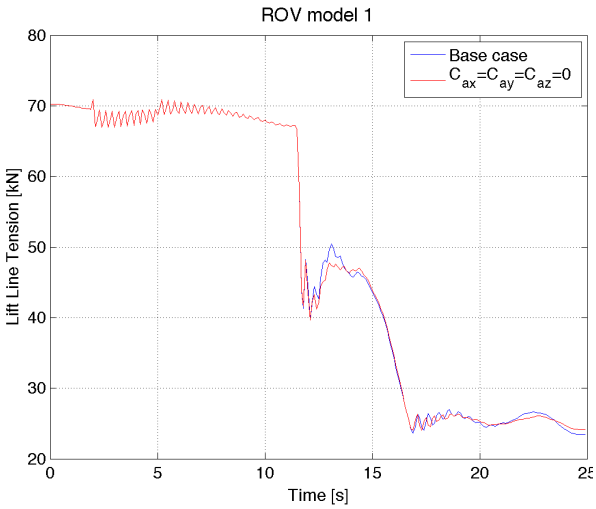

Figure 6.12: ROV 1 - Base case and C_a = 0

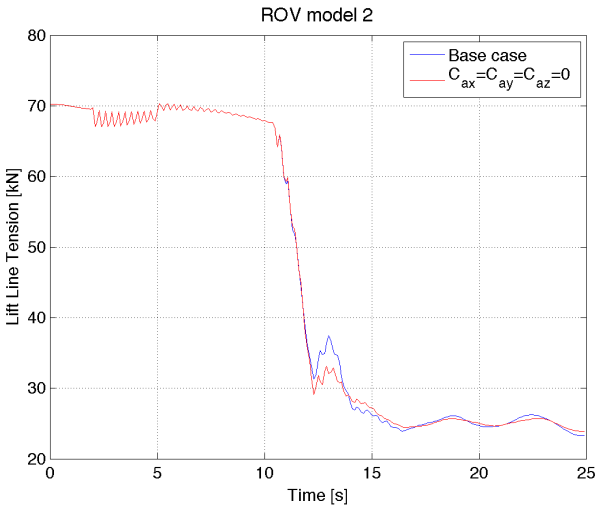

Figure 6.13: ROV 2 - Base case and C_a = 0

Drag coefficient

The drag coefficient for the ROV system has been discussed in Section 3.5.2. Due to the difference in the drag coefficients in the different directions, all coefficients are increased and decreased by 20% for ROV model 1 and 2. The lift line tension due to the variation of the drag coefficients for ROV model 1 and 2 are plotted in Figures 6.15 and 6.15.

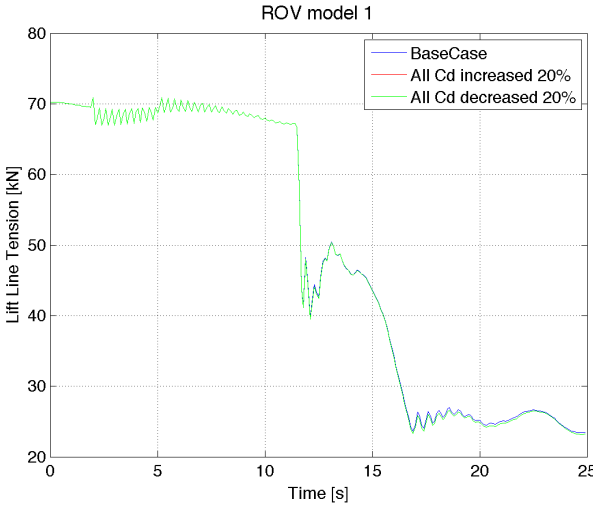

Figure 6.14: ROV 1 - Base case and C_d-range

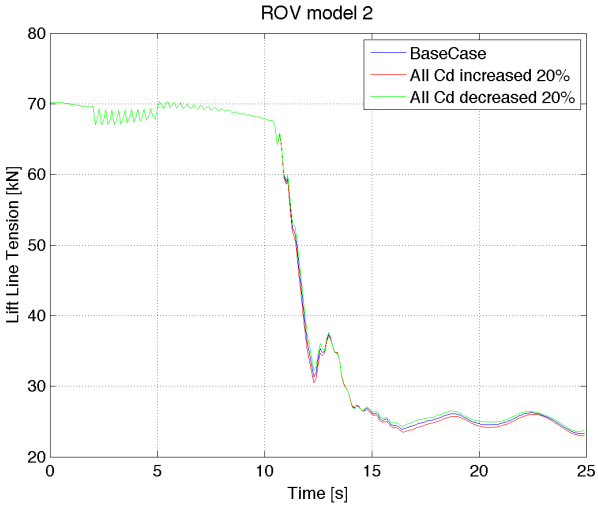

Figure 6.15: ROV 2 - Base case and C_d-range

In the two following figures the drag term is neglected and plotted against the base case for each ROV model.

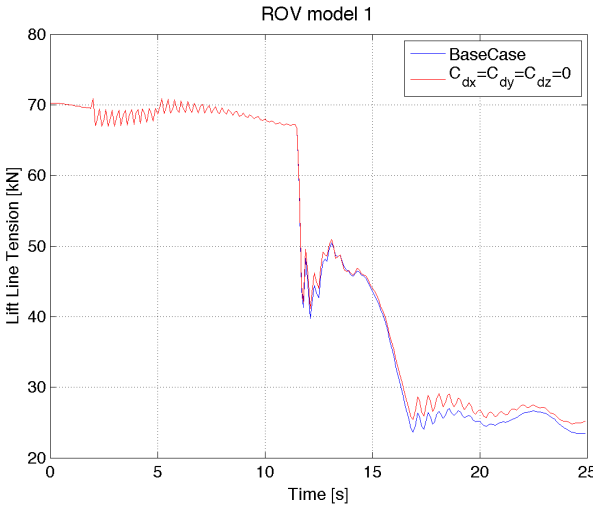

Figure 6.16: ROV 1 - Base case and $C_d = 0$

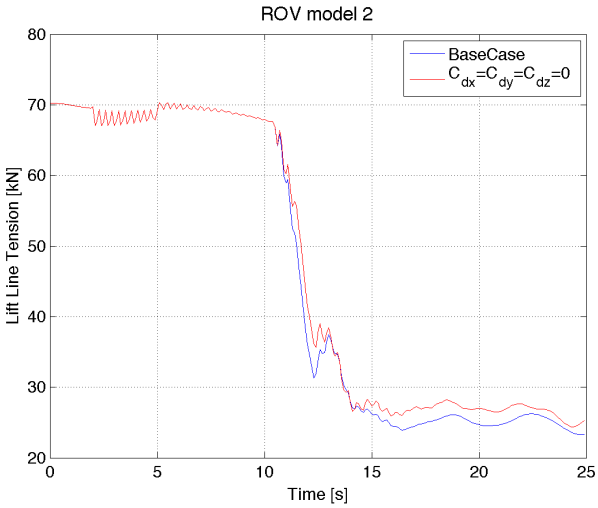

Figure 6.17: ROV 2 - Base case and $C_d = 0$

The sensitivity of the models due to changes in added mass and drag is studied by calculating the maximum deviation in lift line tension compared to the predefined base case. The lift line

tension changes throughout the simulation, and therefore the deviation is calculated for each time instant. The total summary for ROV model 1 and 2 is found in Table 6.3 and is further discussed in Section 7.3.1.

Table 6.3: Maximum deviation in the lift line tension from the defined base case

		Deviation in lift line tension [kN]	
		ROV 1	ROV 2
Added Mass	C_a increased	0.74	1.17
	C_a decreased	0.58	1.02
	C_a neglected	3.07	5.36
Drag	C_d increased	0.43	1.21
	C_d decreased	0.43	1.21
	C_d neglected	2.49	6.07

Added mass and drag coefficient of importance

In the four following figures the added mass and drag coefficient in x, y and z-direction for ROV model 2, have been varied to derive which of the components contribute to added mass and drag effect. In Figure 6.18 C_{ax} and C_{ay} is 0, while C_{az}, the vertical component of added mass is 0.8. It is plotted against the base case where all added mass coefficients are 0.8. In Figure 6.19 three cases are plotted. In the first case C_{ax} = 0.8, while the rest of the coefficients are zero. In the second case C_{ay} = 0.8, while the rest of the components of added mass are zero. In contrast to Figure 6.18 where the tension is compared to the base case where all C_a are 0.8, these two cases are plotted against the case where the added mass contribution is neglected.

The same analyses have been performed for the drag components of ROV model 2. In Figure 6.18, C_{dx} and C_{dy} are zero, while the vertical drag component, C_{dz}, is 0.8. In Figure 6.21, C_{dx} = 0.8 and C_{dy} = 0.8 while the other components are zero. The two cases are plotted against the case where the drag is neglected.

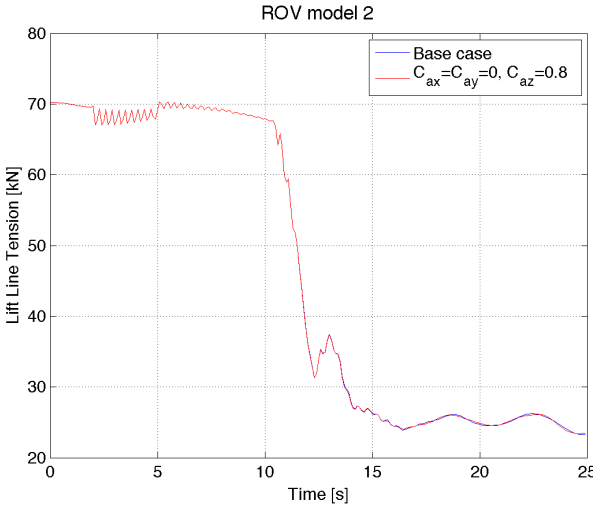

Figure 6.18: Base case and C_{az} = 0.8

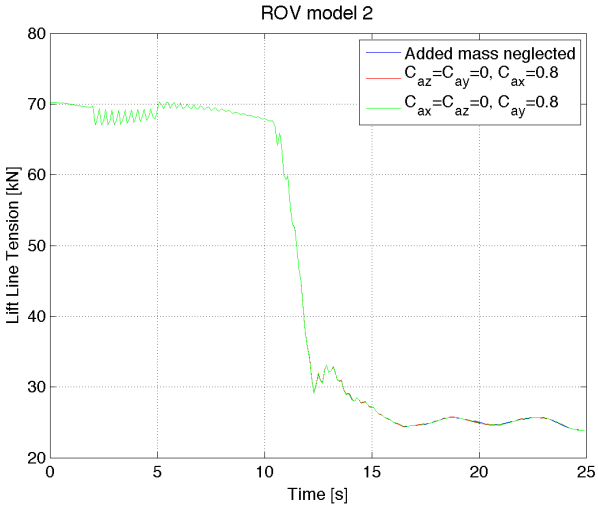

Figure 6.19: C_a neglected, C_{ax} = 0.8, C_{ay} = 0.8

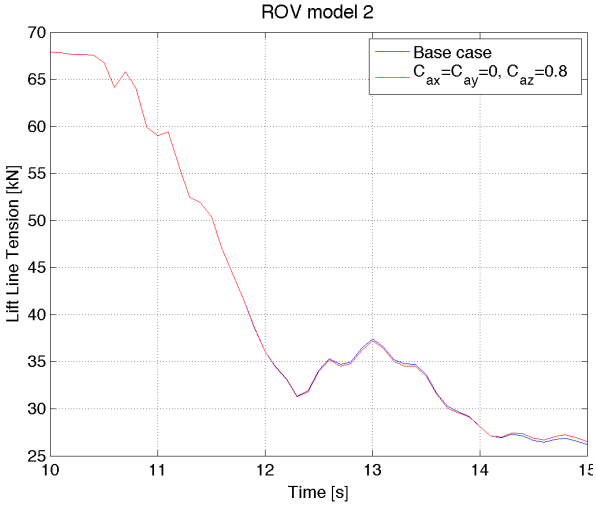

Figure 6.20: Base case and C_{dz} = 2.5

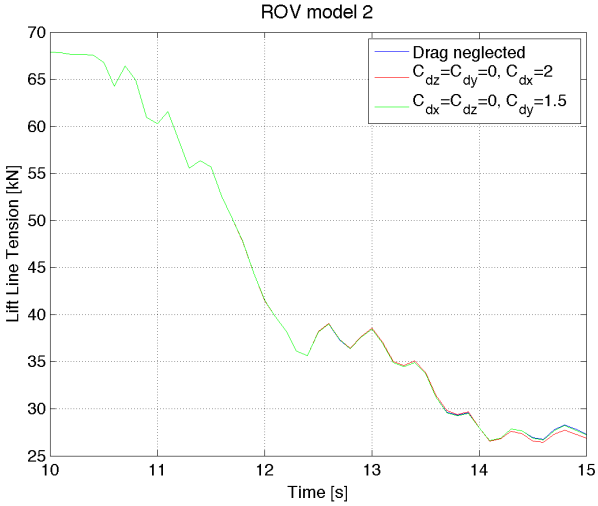

Figure 6.21: C_d neglected, C_{dx} = 0.8, C_{dy} = 0.8

Slamming coefficient

An additional study of the slamming coefficient for the two models has also been performed. In Figures 6.23 and 6.23 the slamming coefficient is neglected and plotted against the previously defined base case. The effect of the slamming coefficient with different modelling techniques is discussed in Section 7.3.1.

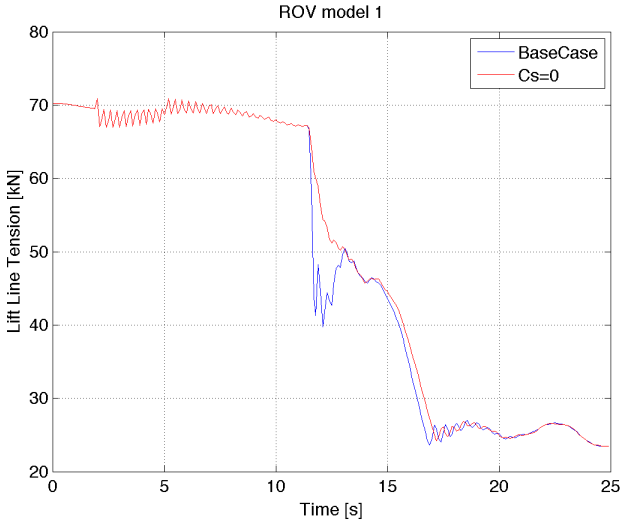

Figure 6.22: ROV 1: Base case and $C_s = 0$

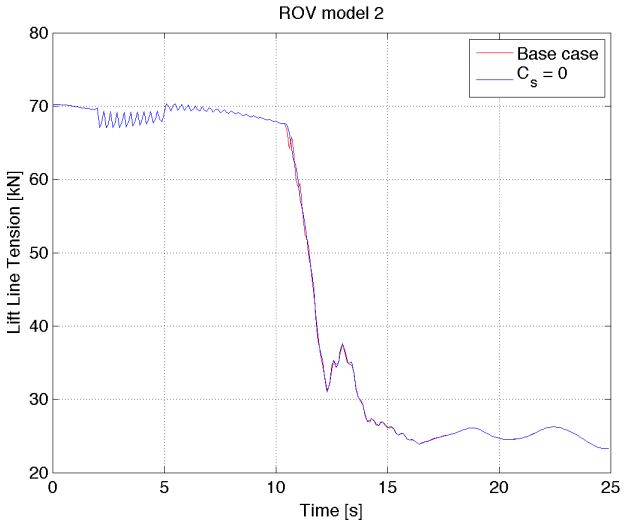

Figure 6.23: ROV 2: Base case and $C_s = 0$

6.3.2 Operational Limit

The procedure of finding an operational limit for the launching and recovery of the ROV system is based on the results discussed in Section 7.2. The discussion concludes that the maximum relative velocity between the vertical components of the crane tip and the wave represents a worst-case scenario. The trend for the maximum relative velocity for varying T_z is shown in Figure 6.24.

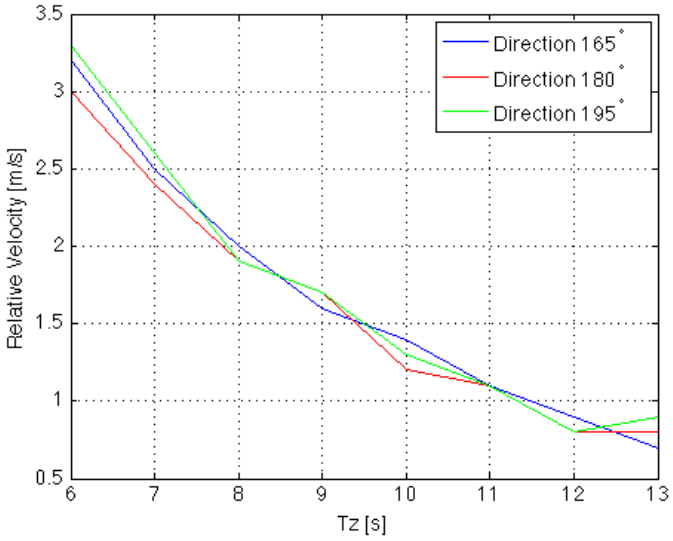

Figure 6.24: Relative velocity between the crane tip and the vertical sea elevation varying with different T_z periods

The sea states investigated in the study of determining the operational limit, are defined by Equation 3.7. The launching operation has been investigated for 3 different seeds, where the maximum relative velocity occurs at different time instants for each seed. The lowering time for different sea states varies with different H_s. The winch is therefore activated 10, 11 and 12 s before the maximum relative velocity occur to ensure that the minimum lift line tension is captured. This results in a total of 1296 simulations. Input for the ROV system are as described by the base case used in Section 6.3.1. The simulations are automated as described in Section 5.3.3. Zero winch tension represents a case where snatch loads in the lifting wire may occur, and is assumed to be an unacceptable sea state for the lowering operation. The minimum lift line tension for all the sea states investigated for ROV model 1 and 2 are included in Appendix F. Operational window for launching is listed in Table 6.4. The T_z values represent the lowest acceptable T_z period to avoid a slack lifting wire.

Table 6.4: Operational window for launching of ROV model 1 and 2

	T_z [s]	
H_s [m]	ROV model 1	ROV model 2
2.5	9	8
3.0	10	9
3.5	11	9
4.0	11	9
4.5	12	9
5.0	12	12

The same simulations are performed for recovery of the ROV system. The ROV system is recovered from a depth of 7 m. The winch is activated at 10, 11 and 12 s before the maximum such that the ROV system is in the wave zone when the maximum relative velocity occurs. Operational window for recovery of the ROV system is listed in Table 6.5.

Table 6.5: Operational window for recovery of ROV model 1 and 2

	T_z [s]	
H_s [m]	ROV model 1	ROV model 2
2.5	6	6
3.0	6	6
3.5	7	7
4.0	8	8
4.5	8	8
5.0	8	8

The scatter diagram included in Appendix B has been used as reference to calculate the probability of experiencing a T_z value lower than a given T_z value, given that the H_s value is known. Only the sea states of interest are included in Table 6.6. Note that the periods are converted to T_z by the relation given in Equation 3.6 and that the H_s values represent the upper limit of the interval.

Table 6.6: Probability of experiencing a T_z lower than a specific value for a given H_s

	$P(T_z<t_z \mid H_s = h_s)$							
H_s [m]	T_z<6	T_z<7	T_z<8	T_z<9	T_z<10	T_z<11	T_z<12	T_z<13
1	54.7	81.9	89.3	93.9	96.6	99.0	99.4	99.7
2	30.4	64.9	77.7	86.6	92.2	97.6	98.7	99.3
3	12.7	46.1	63.3	77.0	86.5	96.0	97.9	99.0
4	3.7	28.2	47.3	65.4	79.4	94.2	97.2	98.7
5	0.7	14.0	31.1	51.7	70.3	92.0	96.4	98.5

6.4 SIMO

The two following figures present the effect of modelling with an additional drag term and the effect of using depth dependent coefficients. A linear and quadratic drag term is used when investigating the effect of the depth dependent coefficients. The simulations are performed in head sea with H_s = 4.5 m and T_p = 11 s, corresponding to a of T_z between 9 and 10 s. To avoid transient effects occurring at the beginning of the simulation, the winch is activated 100 s into the simulations. The winch speed is driven up over time to avoid transient effects influencing the lift line tension in the splash zone.

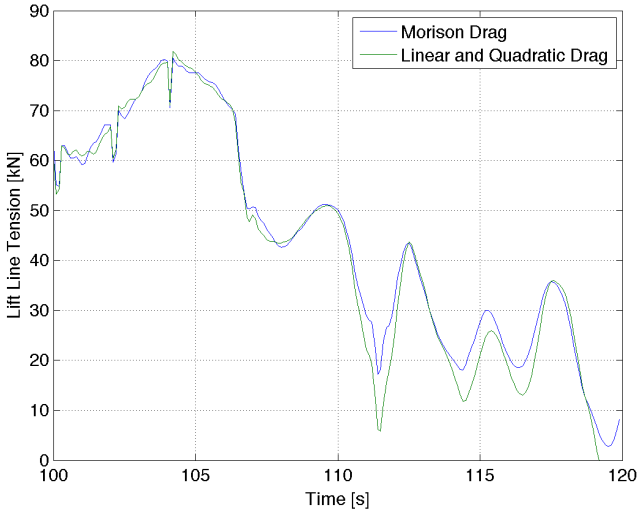

Figure 6.25: Modelling of drag

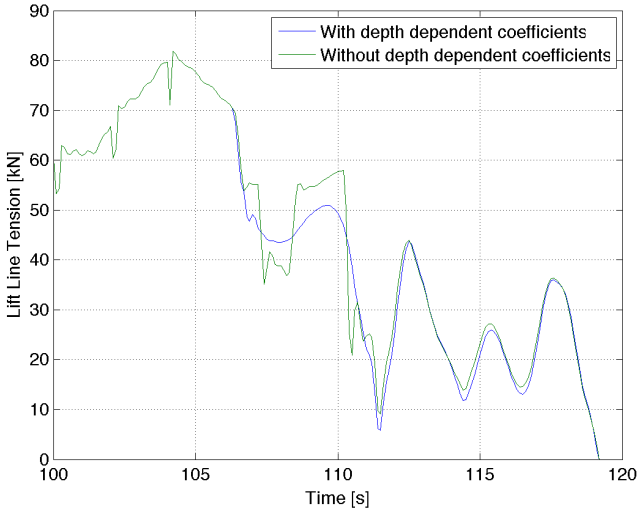

Figure 6.26: Depth dependent coefficients

About 111 s into the simulation shown in Figure 6.25, the additional linear drag term verify its effect. At 106 s into the simulation shown in Figure 6.26 the ROV system interacts with the water and the effect of the depth dependent coefficients is pronounced.

6.4.1 Parameter Variation

The hydrodynamic coefficients for the ROV model in SIMO are also investigated. Linear and quadratic modelling of the drag term is used in the study of parameter variation of the hydrodynamic coefficients used in SIMO. Head sea, H_s = 4.5 m and T_p = 11 s is are environmental parameters used in the simulations. A predefined base case with coefficients listed in Table 6.7 is used as reference for comparison.

Table 6.7: Base case settings

	y	z
C_a	0.8	0.8
b_1	0.3	0.3
b_2	1.95	1.95

Added mass coefficient

Figure 6.27 highlight the changes in the lift line tension due to an increase and decrease of the added mass coefficient. The C_a-range investigated in OrcaFlex is also investigated for the ROV model in SIMO. In Figure 6.28 the added mass coefficient is neglected.

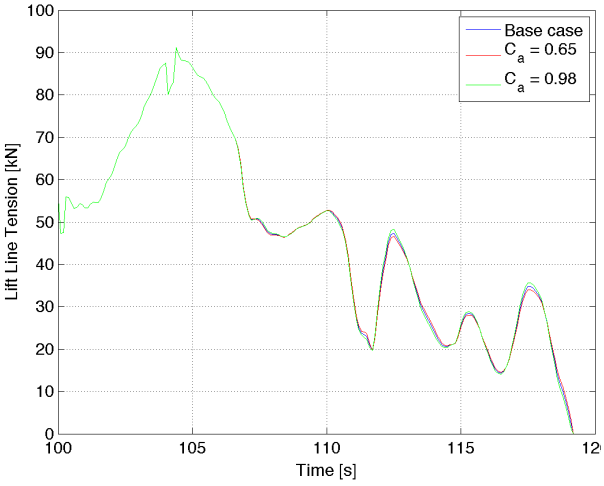

Figure 6.27: Base case and C_a - range

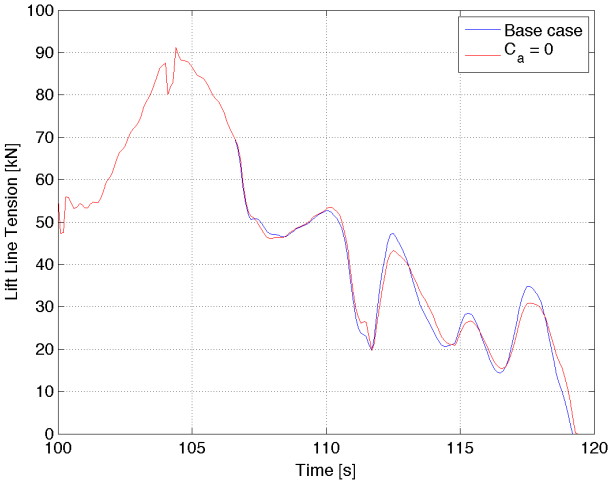

Figure 6.28: Base case and C_a = 0

Drag coefficient

The two following figures show how the lift line tension varies with when the drag coefficient in increased and decreased by 20%. Figure 6.29 illustrate the effect of an increase and decrease of the drag term, and Figure 6.30 presents the difference in the lift line tension when the drag term is completely neglected.

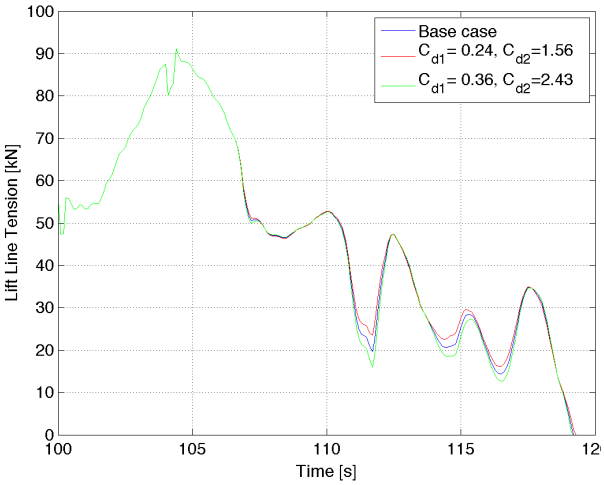

Figure 6.29: Base case and C_d - range

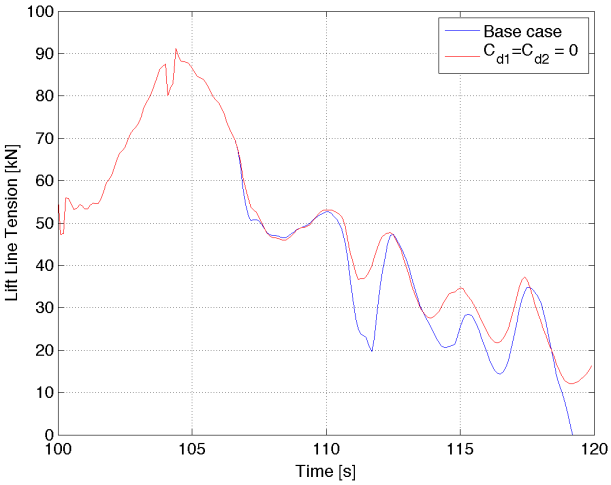

Figure 6.30: Base case and $C_d = 0$

Dependency of added mass and drag coefficient

Table 6.8 summarize the deviation in the lift line tension for each parameter variation case studied. The deviation is given as the maximum lift line difference occurring at a time instant.

Table 6.8: Maximum deviation in the lift line tension from the defined base case

		Deviation in lift line tension [kN]
Added Mass	C_a increased	1.04
	C_a decreased	1.24
	C_a neglected	5.60
Drag	C_d increased	3.77
	C_d decreased	3.78
	C_d neglected	20.22

6.4.2 Operational Limit

As described in Section 5.4, the maximum relative velocity between the crane tip and the distributed dummy element representing the velocity of the wave is computed and post

processed in SIMA.

The simulations are performed such that the ROV system hits the water at the time instant of maximum relative velocity. Similar to the simulations in OrcaFlex, this as also been performed at three different time instants before the maximum relative velocity occurs.

Due to the increased time required for running a three hour simulation in SIMO compared to OrcaFlex, the current operational sea state of H_s = 4.5 m is investigated further. The simulations in SIMA are also more time consuming due to the fact that the automation made possible in OrcaFlex using Python, has not been made possible in SIMO.

Figures 6.31 and 6.32 represent the minimum lift line tension for launching and recovery of the ROV system in a sea state with H_s = 4.5 m.

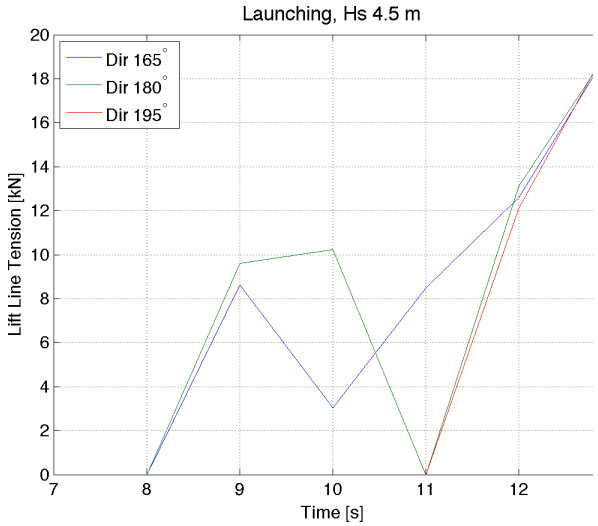

Figure 6.31: Launching, H_s = 4.5 m

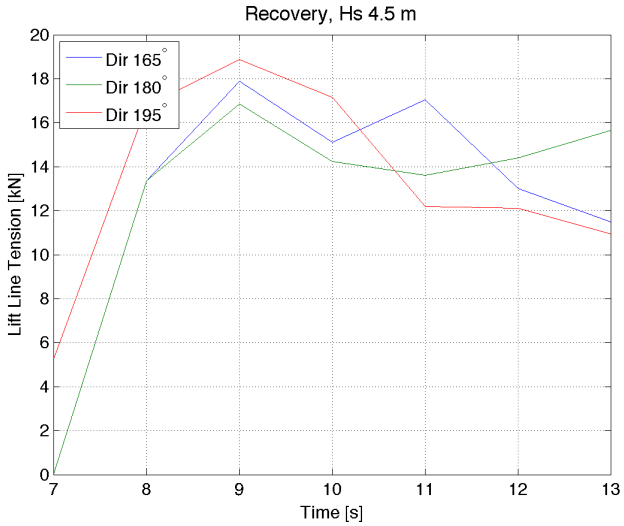

Figure 6.32: Recovery, H_s = 4.5 m

In a three hour sea state with H_s = 4.5 and T_z = 11 s the movement of the crane tip has been studied to detect differences in the vessel motions due to varying direction of incoming wave. Table 6.9 shows the standard deviation of the crane tip elevation and velocity in sea states with different heading angles.

Table 6.9: Standard deviation of crane tip movement with varying direction of incoming wave

	Standard Deviation	
Direction [°]	Position [m]	Velocity [m/s]
165	0.94	0.43
180	0.95	0.43
195	1.01	0.45

7 Discussion of Results

7.1 Analytical Calculations

As described in Section 3.4.2, Equation 3.20 must be fulfilled in order to avoid snap forces in the launching wire. This is used as basis for determining an operational limit for the launching operation of the ROV.

7.1.1 Load Cases

Load Case 1

Only the heave acceleration of the crane tip influences the mass force in load case 1. This is therefore the only contribution to the hydrodynamic force as it is defined in the Simplified Method. The ROV system is not in contact with the water, and there is therefore no contribution from the water particle acceleration. It is observed that the largest crane tip accelerations occur at a T_Z period of 7.0 s in the H_s range 3.5-5.0 m. As seen from Equation 3.25, the mass force is proportional to the heave acceleration when added mass is zero. The hydrodynamic force will therefore be at its largest at the same T_Z period as where the crane tip acceleration is largest. This is seen from Figure 6.1 and 6.3. In the H_s range of 2.5 m to 5 m the accept criteria is valid for load case 1, and no snap forces will occur when the ROV is hanging in the air.

Load Case 2

The ROV system in load case 2 will experience a slamming force acting underneath the ROV. Due to the wave elevation the system will also be exposed to a small varying buoyancy force. As it is seen from Figure 6.4 the hydrodynamic force exceeds the acceptance criteria for sea states with H_s between 2.5 m and 5.0 m. In Appendix C.1 the hydrodynamic force for the lower H_s sea states are plotted for the corresponding T_Z. These results show that the hydrodynamic forces arising for H_s = 1.0 m and below, is within the acceptance criteria limit.

Load case 3

In load case 3 the acceptance criteria is exceeded for all H_s, except sea states with H_s = 0.75 m or less. For the H_s range 2.5-5.0 m the hydrodynamic force is 2-4 times larger than the acceptance criteria, and snap forces may occur in the lifting line. The major hydrodynamic contributions from the ROV come from the mass force and the drag force. For the TMS the largest contribution is due to the varying buoyancy force. The static weight of the system is reduced significantly due to the fact that the ROV is neutrally buoyant in water.

Load case 4

The static weight of the system is additionally reduced when the whole system is submerged in load case 4. A consequence of this is that the acceptance criteria for the pertinent H_s is exceeded. For the lower sea states all T_Z values for H_s = 1.5 m is acceptable, and for H_s = 2 m, T_Z values above 9 s are acceptable. For this load case the drag force and the mass force contribute to the total hydrodynamic force.

7.1.2 Largest hydrodynamic forces

The largest hydrodynamic forces occur in load case 2, where the magnitude of the force is in the region of 300 - 350 kN for H_s = 4.5 m. This may be seen from Figure 6.4. The extreme values of the hydrodynamic force in load case 2 arise due to the slamming forces acting underneath the ROV. In load case 3, the combination of reduced weight and large mass and drag forces is the reason for the accept criteria being exceeded. Due to the fact that the static weight of the system is decreased to the minimum value for load case 4, this load case may be interpreted as the most critical load case. Figure 6.6 show that this is not the case as the hydrodynamic force for load case 4 is significantly smaller than for load case 2. From Equations 3.18 and 3.18 it may be seen that the vertical velocity and vertical acceleration is decreased as the distance to the lowered objects COG is increased. This influences the hydrodynamic forces acting on the object. As load case 2 has considerably larger hydrodynamic forces than the rest of the load cases, this is considered the most critical load case.

7.1.3 Snap Forces

Snap forces are likely to occur for load case 2,3 and 4. The trend observed for the hydrodynamic forces is seen for the snap forces all well, the loads are reduced as the T_Z period increase. For H_s = 4.5 the snap forces lie in the range of 550 - 650 kN for all of the three load cases, where load case 3 have slightly higher values. The calculation of the snap forces are simplified and uncertainties lie in the stiffness of the system and the snap velocity used in the calculation.

7.1.4 Operational limit

The calculations performed according to the Simplified Method clearly reject the present operational H_s of 4.5 m. The acceptance criteria is exceeded for load case 2, 3 and 4 when considering a H_s of 4.5 m. This may cause a slack launching wire, which is not acceptable if the operation is to be carried out according to the relevant standards. If the four load cases are considered as a whole, the limiting H_s would be 0.75 m, originating from load case 3. The approach suggested by DNV utilizes conservative assumptions and significant simplifications, which leads to an overestimation of the hydrodynamic loads acting on the ROV system. The main contributions to the large hydrodynamic forces are the relative velocity and acceleration, where a wave amplitude of $0.9H_s$ is used.

7.2 Worst Case

The lift line tension in Figure 6.7 for the case based on the maximum relative velocity is clearly reduced compared to the case based on the maximum relative acceleration. From Equation 3.14 it is seen that the hydrodynamic loads acting in the splash zone are either velocity dependent or acceleration dependent. The approach of assuming that the maximum relative velocity represents a worst-case scenario is therefore reasonable.

The validation test consolidates the approach of using the maximum relative velocity for finding an operational window for the lifting operation of the ROV system. In contrast to the simulation based on the relative maximum velocity, none of the cases in the random simulations experience zero lift line tension during the lowering through the splash zone. This validation test strengthens the approach of assuming that the maximum relative velocity represents a worst-case scenario. Nevertheless, it is to be noted that there lie uncertainties if the minimum lift line tension is captured if the results are based on one lowering operation. To ensure that the maximum relative velocity is captured, the winch may be activated at different time instants before the maximum relative velocity occurs.

The common practice of performing a large number of simulations to obtain a statistical confidence for many sea states, is very time consuming. In OrcaFlex 144 sea states are investigated with winch activation at three time instants. This results in a total of 432 simulations. If the same simulations are to be performed using the approach of statistical confidence and simulating 100 lowering operations for each sea state, a total of 14 400 simulations would be needed.

The findings made in the study of a worst-case scenario are further used in determining an operational limit in OrcaFlex and SIMO.

7.3 OrcaFlex

Figure 6.9 illustrates the effect of dividing the ROV system into several elements. The rapid reduction of the lift line tension observed for ROV model 1 origin from the simple modelling of buoyancy while the height of the lumped buoy passes through the water surface. By using multiple lumped buoys and a spar buoy in ROV model 2, the buoyancy is treated in a more realistic matter as the lift line tension is gradually reduced throughout the lowering operation. The two lumped buoys representing the ROV allow for stepwise calculation of the hydrodynamic loading through the splash zone. This is assumed to represent a more realistic modelling technique, as loads acting on one part of the ROV system, may not act on other parts of the ROV system.

7.3.1 Parameter Variation

The increase and decrease of C_a for ROV model 1 and 2 has marginal effect on the lift line tension. Nevertheless, the added mass contributions for the two models are emphasized in Figure 6.12 and 6.13, where the base case (blue line) has $C_a = 0.8$, and the second case has $C_a = 0$.

The variation of the drag coefficient shows the same results as for the variation of the added mass term, there is no considerable change in lift line tension within the defined C_d-range. For $C_d = 0$, ROV model 2 shows the largest deviation from the defined base case.

From Table 6.3 it may be seen that ROV model 1 is less sensitive to changes of the hydrodynamic coefficients compared to ROV model 2. The maximum deviation from the defined base case for ROV model 1, arise when the added mass contribution is neglected. The deviation is 3.07 kN when neglecting the added mass, and 2.59 kN when the drag terms are neglected. The difference in the two deviations are minimal, nevertheless, it is concluded that ROV model 1 is inertia dominated. For ROV model 2 the maximum deviation between the two lift line tensions origin from neglecting the drag term, implying that ROV model 2 is drag dominated. The differences originate due to the difference in the ROV models. ROV model 2 is composed of three elements taking the drag effect into account. The three elements represent a more complex geometry than the lumped buoy in ROV model 1, consequently allowing the drag effects to be additionally pronounced.

Figures 6.18 and 6.19 show that the main contribution for the added mass, comes from the added mass in heave direction. Added mass in sway and surge have no impact on the lift line tension during the penetration of the splash zone, and may just as well have been set to zero. The same effect is seen for the drag force. The horizontal components of the drag coefficients do not influence the lift line tension during penetration of the wave zone, and are equal to the case where drag is neglected. The penetration of the wave zone is a vertical dominated motion, and therefore the horizontal effects have no influence on the lift line tension.

Figure 6.22 illustrates the contribution of the slamming coefficient for ROV model 1. The sudden reduce of the lift line tension 11 s into the simulation corresponds to the time instant when the ROV system hits the water. When the slamming effects are neglected, the lift line tension is a continuous curve due to the missing impulse forces. In Figure 6.23 the slamming effect shows little influence on the lift line tension for ROV model 2. Due to the absence of the impulse loading the modelling of four separate slam buoys is questionable.

As described in Section 4.1 the slamming force is only applied while the height of the buoy is passing through the water surface. This means that sufficient time steps are needed to detect the slamming effect of the buoys. If the buoy is above the water in one time step, and fully

submerged in the next time step the slamming effect would be missed. With a lowering speed of 0.5 m/s and a time step of 0.01 s, the ROV system moves 0.005 m per time step. As the slamming buoys are modelled with a height of 0.02 m, four time steps are needed for the buoy to pass the free surface. According to Orcina, (Colin Bludell) this is enough time steps for the slam force to be included in the calculation. If the slam force is calculated for the still water level, ignoring the water particle motions, the slamming force on one buoy would by equal to 0.61 kN. Slamming loads in the range 1.05 -1.15 kN are observed on the four slam buoys, which is consistent to the still water slam force if the water particle motions are taken into account. This implies that the slamming effect is taken into account for ROV model 2. ROV model 2 is therefore considered to represent a more realistic case than ROV model 1.

7.3.2 Operational Limit

The operational limit for a specific H_s value is eminently dependent of the sea state's T_z value. The trend observed in Figure 6.24 may be verified by Equation 3.1. The water particle velocity is inversely proportional to the T_z value. As seen in Appendix F.1 and F.2 the minimum lift line tension is increased for higher T_z values due to the reduction of the relative velocity between the crane tip and the water particles.

For launching of the ROV system, ROV model 2 indicate a wider operational window than ROV model 1. This is believed to originate from the way the two models take buoyancy into account and the difference in the calculation of the slamming forces for the two ROV models. If the sea states are evaluated on an overall basis, an operational T_z value of 12 s is acceptable. From Table 6.6 it is seen that the probability of a T_z lower than 12 s occurring in the North Sea, is very likely, over 96% for all sea states considered.

If ROV model 2 is assumed to represent the most realistic case, the limiting T_z value for the current operational limit of 4.5 m is 9 s. The probability of having this sea state with T_z values lower than 9 s is 52 %. This is far too likely in order to conclude that the sea states with T_z below 9 s may be neglected. The limiting value of T_z = 9 s must therefore be given as additional information for the operational limit.

The two ROV models obtain the same operational limit for recovery. It is observed that the operational limit for the recovery of the ROV system is less conservative than the launching of the system. This is believed to origin due to the reduced water exit coefficient and water exit area of the ROV system. On an overall basis, the lowest acceptable operational T_z value allowed is 8 s. For the lowest sea states with H_s = 2.5 – 3.0 m, T_z = 6 s is acceptable. The probability of experiencing sea states with T_z values less than 6 s for H_s = 2.5 – 3.0 m, is 12.7 %. This is also a considerable high probability, meaning that the lower sea states also should be given with a limiting T_z value.

7.4 SIMO

In Figure 6.25 the effect of an additional linear drag term is compared to the quadratic drag as used in Morison's equation. The effect of the linear drag is visible from about 111 s into the simulation. This represents the time instant when the ROV is fully submerged. The lift line tension is significantly reduced due to the additional drag term, even though it is low compared to the quadratic term. The linear coefficient is only 0.3, compared to the quadratic coefficient of 1.95. The additional effect of the linear drag term is in compliance to the findings achieved by Øritsland and Lehn (1987) as described in Section 3.5.2.

The effect of the depth dependent coefficients for the slender elements is illustrated in Figure 6.26. The influence of the depth dependent coefficients is visible at 108 - 110 s into the simulation. This is the time instant of the ROV's interaction with the water surface. It may be seen that the depth dependent coefficients model a smooth penetration through the splash zone. For the case without the depth dependent coefficients, the lift line tension is discontinuous. Horizontal slender elements without depth dependent coefficients are either fully submerged or totally out of the water. Due to this rapid change of buoyancy and hydrodynamic forces the lift line tension changes unreasonably fast for the case without depth dependent coefficients. The added mass and drag coefficients are highly dependent on the proximity to the free surface, which may be seen in Figure 3.3. Even though the object is fully submerged, its full effect of the added mass does not have an effect until the element is submerged a depth of three times its radius. Allowing for depth dependent coefficients therefore models the penetration through the splash zone more realistic than without depth dependent coefficients. The depth dependent coefficients for the drag term are uncertain as these are taken as the ratio of the relative submerged volume.

7.4.1 Parameter Variation

From Table 6.8, the change of added mass within the C_a range is observed to have a limited effect on the lift line tension. The large deviations in the lift line tension due to neglecting of the drag term indicate that the ROV-system is drag dominated. The dependency of the drag term originates from the slender elements used in the modelling. Modelling the system with a too high drag term, may lead to excessive unrealistic, damping of the ROV. As the depth dependent drag coefficients are assumed equal to the ratio of the relative submerged volume, it should be noted that there lies uncertainties in the results implying that the structure is drag dominated. In 6.30 it is may be seen that the base case modelled with drag represent a conservative case as the lift line tension becomes slack for this case, and not the case modelled without the drag term.

7.4.2 Operational Limit

Only the current operational sea state of H_s = 4.5 m is investigated in SIMO. The lowest allowable T_z value for launching is 12 s. As for OrcaFlex, this signify that the operational sea state should limited with a T_z value, as well as a H_s value. The probability of experiencing a sea state with zero-up crossing periods less than 12 s for a sea state with H_s = 4.5 m is 96.4 %. This implies that if the operation is performed independent of T_z value, a slack lifting wire would occur 96.4 % of the time, assuming that the maximum relative velocity occurs.

Similar to the results in OrcaFlex, recovery of the ROV system allows a wider operational window. This implies that for the current operational limit for the ROV, the lifting wire is likely to become slack for T_z values less than 8 s. The probability that a sea state with H_s = 4.5 m, will have T_z values less than 8 s is 31.1 %. The difference in the T_z indicates that different operational limits should be set for lowering and recovery of the ROV system.

When the waves approach the vessel ±15° of vessel heading additional roll motions may provide increased movement of the crane tip. Table 6.9 shows that the crane tip movement is slightly larger for waves of direction 195 °. This is the case when the waves approach the vessel from the same side as the ROV is lowered. However, No clear trend of the heading angles are observed when analysing the operational limit for the ROV system.

7.5 Comparison

The present operational sea state of H_s = 4.5 m is clearly rejected by the analytical calculations performed according to the Simplified Method. The results indicate that an operational H_s of 0.75 m is acceptable for launching of the ROV, if it is to be performed independent of T_s value.

From the time domain analyses in SIMO and OrcaFlex, the current operational sea state of H_s = 4.5 m could be justified if a limiting T_s value is given. For OrcaFlex the limiting value is 9 s. In SIMO the limiting value is 12 s. This is the same for ROV model 1. Recovery of the ROV system is limited by T_s = 8 s for all three ROV models. This indicates that the differences in the ROV modelling are most prone to launching of the ROV system. The large deviations in the operational limit achieved from analytical calculations and the time domain simulations indicate that the Simplified Method does indeed result in a restrictive operational window.

Although the main dimensions of the models used in the different analyses are the same, they differ in the way they are modelled. This includes number of objects used, geometry of the model and the modelling of drag in SIMO. The deviations in the modelling may also be seen in the results.

The three different ROV show different dependency of the added mass and drag term. As described in Section 3.5.1, an increased perforation gives a reduction of the added mass of the object and an increase of the drag contribution. The trend observed is drawn to the findings achieved by Kopsov and Sandvik (1995) and Sandvik et al. (1993). ROV model 1 is modelled as a lumped buoy, which may be associated to a box without perforation. This model is concluded to be inertia dominated. ROV model 2 is composed of several buoys, allowing hydrodynamic contributions to be generated for each buoy. Dividing up the system also allows for a perforation effect, at least for the hollow spar buoy representing the TMS. The drag term is dominating for this model. The last ROV model composed of 48 slender elements is highly perforated, and as the results show, the model is drag dominated.

It may be argued that the ROV model from SIMO induce conservative results regarding a slack launching wire. This is based upon the fact that the operational window obtained in SIMO, is the same as the operational window obtained for the simplest ROV model in OrcaFlex. The simplest model in OrcaFlex, ROV model 1, is assumed to model unrealistic results due to the simple treatment of buoyancy. In addition, the ROV model in SIMO is highly drag dependent due to the slender elements making up the model. There exist uncertainties associated with a high drag because of the unrealistic damping that may be induced. If the vessel moves in heave the ROV system will follow the vessel motions upwards, but not necessarily downwards due to dampened motions of the ROV in water. With an unrealistically high damping, the duration of the time interval of a slack lifting wire is increased.

The main differences between OrcaFlex and SIMO are related to the modelling and the calculation of the forces on the ROV system. In SIMO, the slamming effect is taken into account only if depth dependent coefficients are given for the slender element. In OrcaFlex, this is given by a slamming coefficient and a corresponding slamming area. The slender elements in SIMO also allow for a linear drag term, which is convenient for problems in the splash zone. It is observed that the variations in the lift line tension for the ROV model in SIMO are larger than the variations in the lift line tension for the ROV models in OrcaFlex. Which of the two representing the most realistic case should be compared to model tests before a specific conclusion can be drawn.

8 Conclusion

The main goal of this thesis was to investigate a lifting operation of a ROV system through the splash zone. The Recommended Practice proposed by DNV for lifting through the splash zone has been used as basis for the analytical calculations. The ROV system investigated in this thesis has also been modelled and analysed in the two time domain programs SIMO and OrcaFlex.

Three different ROV models have been established, two in OrcaFlex and one in SIMO. There exist uncertainties associated with the hydrodynamic coefficients chosen for the ROV models. Parametrical studies of the ROV system have been performed for each model. The overall observations conclude that small variations of the hydrodynamic coefficients do not affect the hydrodynamic forces in a significant matter. However, the importance of the hydrodynamic coefficients is pronounced when they are neglected in the analyses. For ROV model 2 in OrcaFlex, studies show that the vertical component of the hydrodynamic coefficients is the main contributor to the hydrodynamic forces. The horizontal coefficients show no effect on the hydrodynamic forces, and the lift line tension is equal to the case where all the hydrodynamic coefficients are neglected. Whether the ROV model is inertia dominated or drag dominated is dependent on the modelling method of the system. The ROV model from OrcaFlex with one lumped buoy is inertia dominated, while the ROV model from OrcaFlex modelled with multiple buoys is slightly more drag dominated. The ROV model in SIMO composed of slender elements is highly drag dependent. For perforated structures compared to solid structures, the added mass dependence is reduced, while the drag dependence is increased. These findings are in compliance with existing published work.

Obtaining an allowable operational sea state by the use of maximum relative velocity between the crane tip and the vertical velocity of the water velocity has concluded to be an efficient alternative, at least when automated, compared to simulating numerous analyses for statistical confidence. It may also be used as a preliminary study for establishing an operational sea state based on statistical confidence.

The Simplified Method is certainly conservative compared to time domain simulations performed in SIMO and OrcaFlex. The present operational sea state of H_s = 4.5 m is rejected by the Simplified Method. If the operation is to be performed independent of a T_s value, an operational H_s of 0.75 m is acceptable for launching of the ROV. From the time domain analyses in SIMO and OrcaFlex, the current operational sea state of H_s = 4.5 m could be justified if a limiting T_s of 9 s value is given. This is based on the assumption that ROV model 2 in OrcaFlex represents the most realistic case of the three ROV models investigated. For

recovery of the ROV system, a limiting T_z value of 8 s, independent of ROV model, is sufficient. The operational limit should not only be set by a H_s value, but also a T_z due to the large dependence of the wave period for lifting though the splash zone.

9 Recommendations for Further Work

The vessel's motions are described by the first order transfer functions. This means that the shielding effect of the vessel is not included. The waves act on the ROV system as if the vessel is not present. The shielding effect of the vessel may reduce the hydrodynamic loading significantly. In addition, the vessel generates radiated waves that may affect the lowering operation of the ROV system. These effects may be captured by establishing data of the vessel in a diffraction program like WADAM or WAMIT. Extended information of the vessel's motions is highly relevant for simulations of heavy lift operations.

The ROV models used in the analytical calculations and in the time domain simulations are simplified, and there lies uncertainties in the estimation of the hydrodynamic coefficients for the ROV system. Model tests or computational fluid dynamic (CFD) analyses of the ROV system would lead to a greater accuracy of the hydrodynamic coefficients used in the analytical calculations and the time domain simulations.

A detailed investigation of the wave kinematics used in the software programs should be established to detect if this has an impact of the results.

The automation made possible in OrcaFlex should also be implemented for SIMO for higher efficiency when generating results. This may be done using MATLAB.

Installation of measuring tools to log the lift line tension during the lowering of the ROV system would be of great interest for comparison of the results obtained from the time domain simulations. In order to enable such a comparison, the sea state also need to be evaluated.

References

Colin Bludell, O. OrcaFlex Support. Mail.

DNV (2010). *DNV-RP-C205 "Environmental Conditions and Environmental Loads"*. Det Norske Veritas AS.

DNV (2011). *DNV-RP-H103 "Modelling and Analysis of Marine Operations"*. Det Norske Veritas AS.

Faltinsen, O. M. (1990). *Sea Loads on Ships and Offshore Structures*. Cambridge Ocean Technology Series. Cambridge University Press.

Kopsov, I. E. and Sandvik, P. (1995). Analysis of subsea structure installation. In *Fifth International Offshore and Polar Engineering Conference*, volume 1.

Lien, H. V. (2009). Response Amplitude Operators, ST-254CD "Edda Flora".

MARINTEK (2013a). *SIMO - Theory Manual*. Norwegian Marine Technology Research Institute, 4 edition.

MARINTEK (2013b). *SIMO - User's Manual*. Norwegian Marine Technology Research Institute, 4 edition.

Nomoto, M. and Hattori, M. (1986). A Deep ROV "Dolphin 3K": Design and Performance Analysis. *Journal of Ocean Engineering*.

Orcina (2013). *OrcaFlex Manual, Version 9.6a*. Orcina Ltd.

Øritsland, O. (1989). A Summary of Subsea Module Hydrodynamic Data. Marine Operations - Crane Operations.

Øritsland, O. and Lehn, E. (1987). Hydrodynamic Forces on Subsea Modules During Lifting Operations. In *Third International Symposium on Practical Design of Ships and Mobile Units*, volume 1.

Øritsland, O. and Lehn, E. (1989). Hydrodynamic Forces and Resulting Motion of Subsea Modules During Lifting in the Splash Zone. In *Eight International Conference on Offshore Mechanics and Arctic Engineeringh International Conference on Offshore Mechanics and Arctic Engineering*, volume 2.

Sandvik, P., Lieng, J., and Lunde, S. (1993). Analysis of the dynamics during installation of subsea structures. In *Offshore 93: Installation of Major Offsjore Structures*, volume 105.

Sarkar, A. and Gumestad, O. T. (2010). Splash zone lifting analysis of subsea structures. In *ASME 2010 29th International Conference on Ocean, Offshore and Arctic Engineering*, pages 303–312. American Society of Mechanical Engineers.

Sayer, P. (1996). Hydrodynamic Forces on ROVs near the Air-Sea Interfacenterface. *International Journal of Offshore and Polar Engineering*, 6.

Sayer, P. (2008). Hydrodynamic Loads During the Deployment of ROVs. *Ocean Engineering*.

Thurson, K. W., Swanson, R. C., and Kopp, F. (2011). Statistical characterization of slacking and snap loading during offshore lifting and lowering in a wave environment. In *ASME: 30th International Conference on Ocean, Offshore and Arctic Engineering*, volume 1.

A ROV and TMS

A.1 Drawings

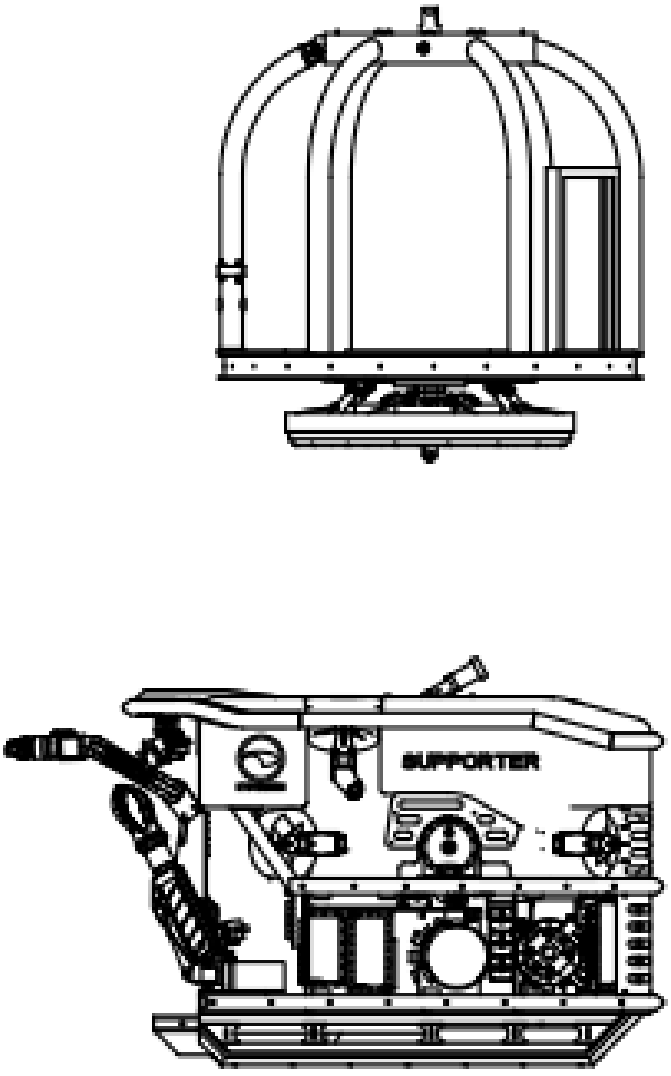

Figure A.1: Drawings of the TMS and the ROV

A.2 ROV input

Excel: ROVinput.xls

B Scatter Diagram

Hs \ Tp	3	4	5	6	7	8	9	10	11	12	13	14	15	16	17	18	19	21	22	Sum
1	59	403	1061	1569	1634	1362	982	643	395	232	132	74	41	22	12	7	4	2	2	8636
2	9	212	1233	3223	5106	5814	5284	4102	2846	1821	1098	634	355	194	105	56	30	16	17	32155
3	0	8	146	831	2295	3896	4707	4456	3531	2452	1543	901	497	263	135	67	33	16	15	25792
4	0	0	6	85	481	1371	2406	2960	2796	2163	1437	849	458	231	110	50	22	10	7	15442
5	0	0	0	4	57	315	898	1564	1879	1696	1228	748	398	191	84	35	13	5	3	9118
6	0	0	0	0	3	39	207	571	950	1069	885	575	309	142	58	21	7	2	1	4839
7	0	0	0	0	0	2	27	136	347	528	533	387	217	98	37	12	4	1	0	2329
8	0	0	0	0	0	0	2	20	88	197	261	226	138	64	23	7	2	0	0	1028
9	0	0	0	0	0	0	0	2	15	54	101	111	78	39	14	4	1	0	0	419
10	0	0	0	0	0	0	0	0	2	11	30	45	39	22	8	2	1	0	0	160
11	0	0	0	0	0	0	0	0	0	2	7	15	16	11	5	1	0	0	0	57
12	0	0	0	0	0	0	0	0	0	0	1	4	6	5	2	1	0	0	0	19
13	0	0	0	0	0	0	0	0	0	0	0	1	2	2	1	0	0	0	0	6
14	0	0	0	0	0	0	0	0	0	0	0	0	0	1	0	0	0	0	0	1
15	0	0	0	0	0	0	0	0	0	0	0	0	0	0	0	0	0	0	0	0
Sum	68	623	2446	5712	9576	12799	14513	14454	12849	10225	7256	4570	2554	1285	594	263	117	52	45	1E+05

Figure B.1: Scatter Diagram

C Results form Analytical Calculations

C.1 Hydrodynamic Force for Low H_s

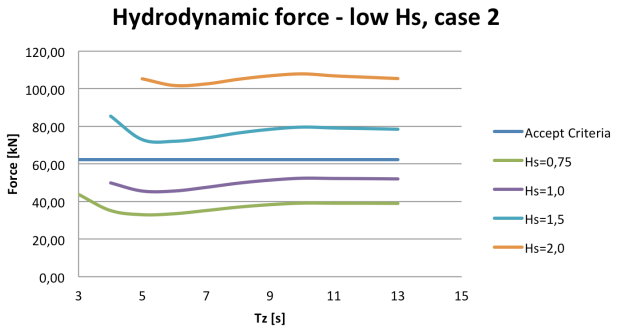

Figure C.1: Hydrodynamic force for load case 2

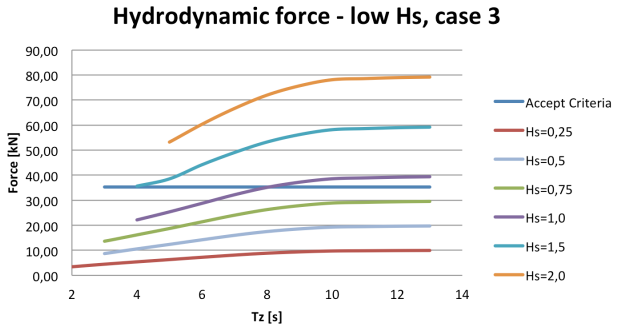

Figure C.2: Hydrodynamic force for load case 3

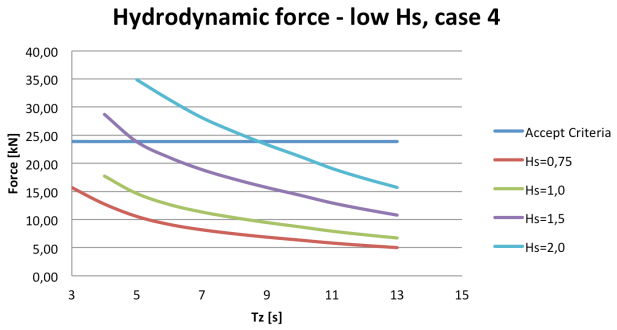

Figure C.3: Hydrodynamic force for load case 4

C.2 Snap Forces

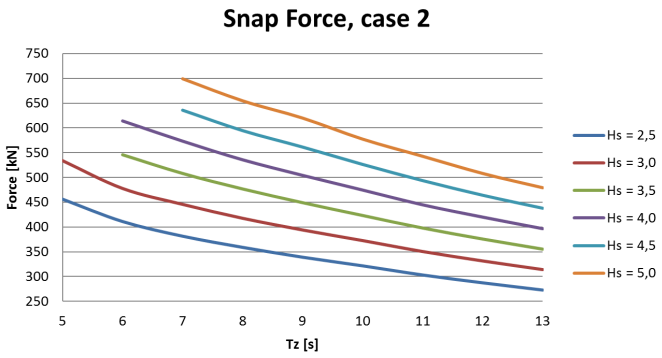

Figure C.4: Snap forces, load case 2

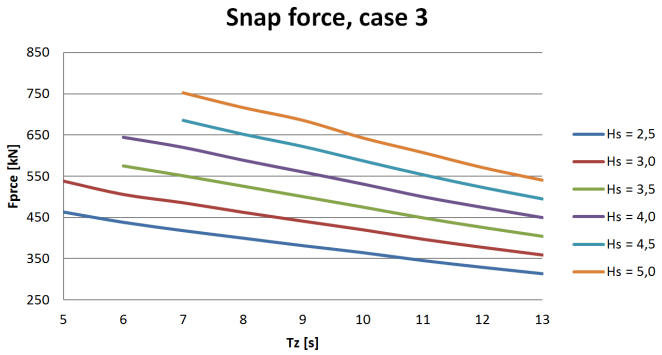

Figure C.5: Snap forces, load case 3

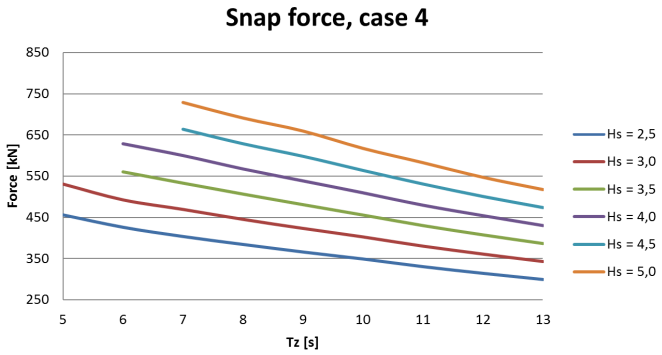

Figure C.6: Snap forces, load case 4

D Vessel Motions in SIMO

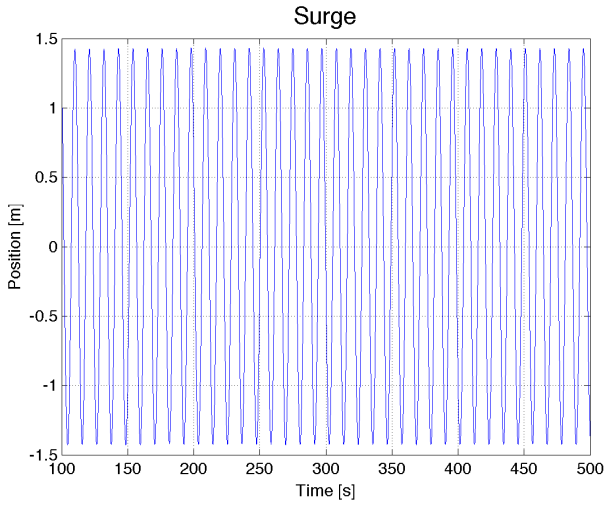

Figure D.1: Surge motion

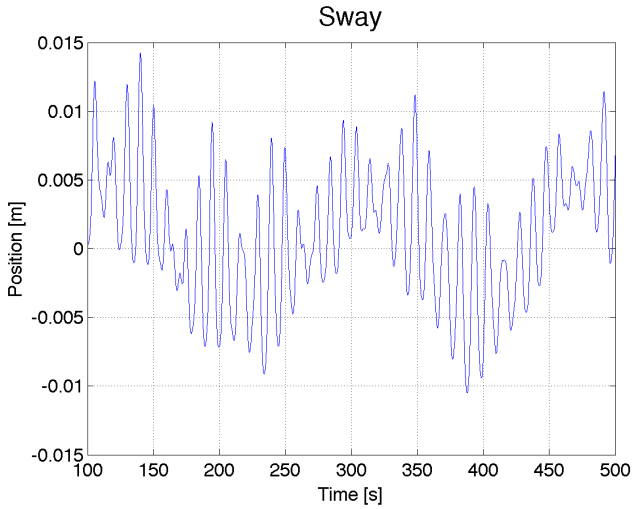

Figure D.2: Sway motion

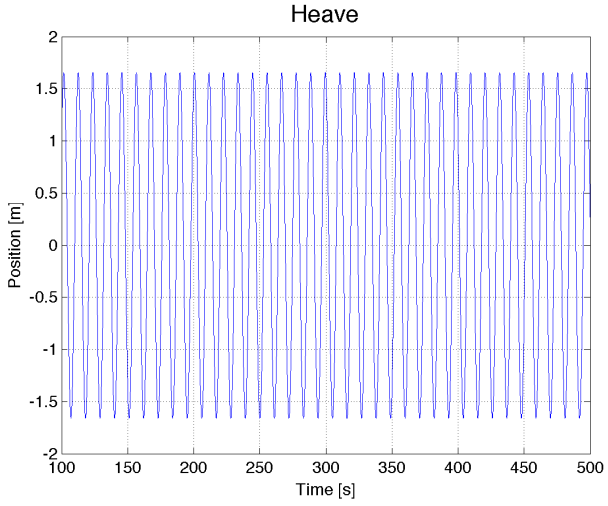

Figure D.3: Heave motion

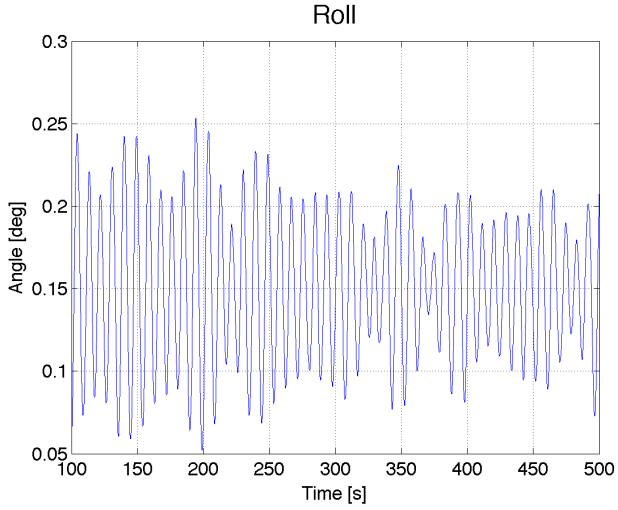

Figure D.4: Roll motion

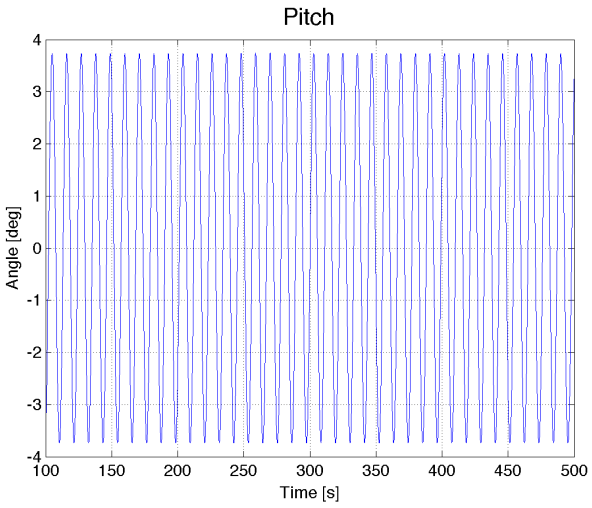

Figure D.5: Pitch motion

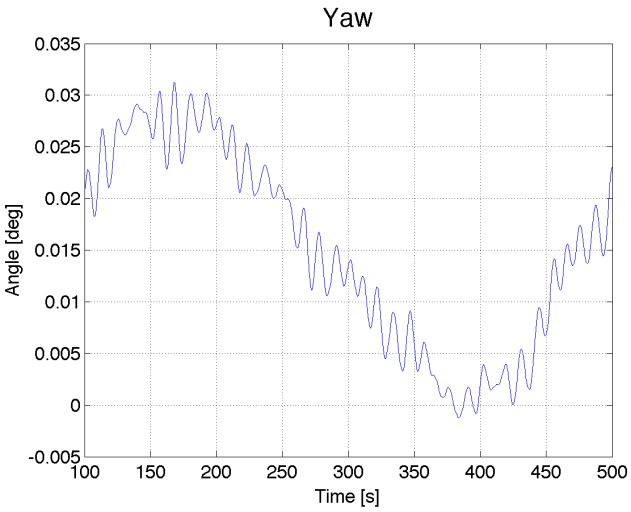

Figure D.6: Yaw motion

E Python script

E.1 Relative Velocity

```
from glob import glob
import os
import csv
import OrcFxAPI
import xlwt

Casenumber = 0

wb = xlwt.Workbook()
ws = wb.add_sheet('Max Relative Velocity')
ws.write(0, 0, 'Casenumber')
ws.write(0, 1, 'Wave Direction')
ws.write(0, 2, 'Wave Height')
ws.write(0, 3, 'Wave Period')
ws.write(0, 4, 'Max Relative Velocity')
ws.write(0, 5, 'Time Instant')

sim_files_list = glob(os.path.join('C:\Users\Rbjerkholt\Documents\Skole\Master\Orcaflex\
    Master\ROVlifting\AllSeaStates\RelativeVelocityCases', '*.sim')) #
for sim_file in sorted(sim_files_list):
    Casenumber = Casenumber + 1
    print "Case", Casenumber

    #Run a 3 hour simulation to find the maximum relative
    model = OrcFxAPI.Model(sim_file)
    crane = model['Crane tip']
    environment = model['Environment']

    Direction = environment.GetData('WaveDirection',0)
    Hs = environment.GetData('WaveHs',0)
    Tz = environment.GetData('WaveTz', 0)

    time1 = model.SampleTimes(OrcFxAPI.Period(1))
    time2 = model.SampleTimes(OrcFxAPI.Period(2))
    time3 = model.SampleTimes(OrcFxAPI.Period(3))

    times = time1 + time2  + time3
    MaxRelVelocity = float('-inf')
    CorrTime = float('-inf')
```

```
#Plotting the relative velocity against the simulation time
filename = 'C:\Users\Rbjerkholt\Documents\Skole\Master\Orcaflex\Master\ROVlifting\
    AllSeaStates\RelativeVelocity\RelativeVelocityCase%.3d.txt' %Casenumber
with open(filename, 'wb') as f:
    writer = csv.writer(f)
    writer.writerow(('time', 'RelVelocity'))

    #Largest relative velocity between the wave and the crane tip
    for time in times:
        period = OrcFxAPI.SpecifiedPeriod(time, time)
        CraneTipVelocity = crane.TimeHistory('GZ-Velocity', period)[0]
        X = crane.TimeHistory('X', period)[0]
        Y = crane.TimeHistory('Y', period)[0]
        SeaZVelocity = environment.TimeHistory('Z Velocity', period, OrcFxAPI.
            oeEnvironment(X, Y, OrcFxAPI.OrcinaDefaultReal()))[0]

        RelVelocity = abs(SeaZVelocity-CraneTipVelocity)
        if RelVelocity > MaxRelVelocity:
            MaxRelVelocity = RelVelocity
        writer.writerow((time, RelVelocity))

    #Time corresponding to the largest relative velocity between the wave and the
        crane tip
    for time in times:
        period = OrcFxAPI.SpecifiedPeriod(time, time)
        CraneTipVelocity = crane.TimeHistory('GZ-Velocity', period)[0]
        X = crane.TimeHistory('X', period)[0]
        Y = crane.TimeHistory('Y', period)[0]
        SeaZVelocity = environment.TimeHistory('Z Velocity', period, OrcFxAPI.
            oeEnvironment(X, Y, OrcFxAPI.OrcinaDefaultReal()))[0]

        RelVelocity = abs(SeaZVelocity-CraneTipVelocity)
        if RelVelocity == MaxRelVelocity:
            CorrTime = time

ws.write(Casenumber, 0, Casenumber)
ws.write(Casenumber, 1, Direction)
ws.write(Casenumber, 2, Hs)
ws.write(Casenumber, 3, Tz)
ws.write(Casenumber, 4, MaxRelVelocity)
ws.write(Casenumber, 5, CorrTime)
wb.save('ResultsRelativeVelocitySeed3.xls')
f.close()
```

E.2 Start Winch

```
import xlrd
import math
#Excel file with results of the time instant where the max relative velocity occurs
file_location = "C:/Users/Rbjerkholt/Documents/Skole/Master/Orcaflex/Master/ROVlifting/
    AllSeaStates/ResultsRelativeVelocity.xls"
workbook = xlrd.open_workbook(file_location)
sheet = workbook.sheet_by_index(0)

stage0 = float('-inf')
stage1 = float('-inf')
stage2 = float('-inf')
stage3 = float('-inf')
stage4 = float('-inf')
num_rows = sheet.nrows

#Definition of variables
WaveDirection = [165, 180, 195] #3 wave directions
WaveHs = [2.5, 3.0, 3.5, 4.0, 4.5, 5.0] #6 different significant wave heights

#Loop for each variation
casenumber_seastate = 0 #used in filename
for Direction in WaveDirection:
    for WaveHeight in WaveHs:
        if WaveHeight == 2.5:
            WaveTz = [5, 6, 7, 8, 9, 10, 11, 12, 13]
        if WaveHeight == 3.0:
            WaveTz = [5, 6, 7, 8, 9, 10, 11, 12, 13]
        if WaveHeight == 3.5:
            WaveTz = [6, 7, 8, 9, 10, 11, 12, 13]
        if WaveHeight == 4.0:
            WaveTz = [6, 7, 8, 9, 10, 11, 12, 13]
        if WaveHeight == 4.5:
            WaveTz = [7, 8, 9, 10, 11, 12, 13]
        if WaveHeight == 5.0:
            WaveTz = [7, 8, 9, 10, 11, 12, 13]
        for Period in WaveTz:
            casenumber_seastate = casenumber_seastate + 1
            for row in range(1, num_rows):
                casenumber = sheet.cell_value(row , 0)
                time_instant = sheet.cell_value(row , 5)
                if casenumber == casenumber_seastate:

                    #duration of stages in sec
                    stage0 = 13
                    stage1 = time_instant - 13   #Start simulation 13 sec before the
                        impact
```

```
stage2 = 3
stage3 = 20

#number of stages-->3
#create individual yml (text) files which are all run in a batch
filename = 'C:\Users\Rbjerkholt\Documents\Skole\Master\Orcaflex\
    Master\ROVlifting\AllSeaStates\StartWinch\Case%.3d.yml' %
    casenumber
f = open(filename, 'w')
# The content of the file:
print >>f, 'BaseFile: C:\Users\Rbjerkholt\Documents\Skole\Master\
    Orcaflex\Master\ROVlifting\AllSeaStates\LiftingAnalysis_ROV.dat'
print >>f, 'General:'
print >>f, '     NumberOfStages:', 3
print >>f, '     StageDuration[1]:', stage0
print >>f, '     StageDuration[2]:', stage1
print >>f, '     StageDuration[3]:', stage2
print >>f, '     StageDuration[4]:', stage3
print >>f, 'Environment: '
print >>f, '     WaveDirection: ', Direction
print >>f, '     WaveHs:', WaveHeight
print >>f, '     WaveTz: ', Period
f.close()
```

E.3 Lift Line Tension

```
from glob import glob
import os
import csv
import OrcFxAPI
import xlwt

Casenumber = 0

wb = xlwt.Workbook()
ws1 = wb.add_sheet('Lift line tension')
ws1.write(0, 0, 'Casenumber')
ws1.write(0, 1, 'Direction')
ws1.write(0, 2, 'Hs')
ws1.write(0, 3, 'Tz')
ws1.write(0, 4, 'MaxTension')
ws1.write(0, 5, 'MinTension')

sim_files_list = glob(os.path.join('C:\Users\Rbjerkholt\Documents\Skole\Master\Orcaflex\
    Master\ROVlifting\AllSeaStates ROV 2\Lifting\StartWinchSeed3_12s', '*.sim'))
for sim_file in sorted(sim_files_list):
    Casenumber = Casenumber + 1
    print "Case", Casenumber
```

```
model = OrcFxAPI.Model(sim_file)
environment = model['Environment']
winch = model['Winch1']

Direction = environment.GetData('WaveDirection',0)
Hs = environment.GetData('WaveHs',0)
Tz = environment.GetData('WaveTz', 0)

time1 = model.SampleTimes(OrcFxAPI.Period(1))
time2 = model.SampleTimes(OrcFxAPI.Period(2))
time3 = model.SampleTimes(OrcFxAPI.Period(3))
times = time1 + time2 + time3

MaxTension = -float('inf')
MinTension = float('inf')

for time in time3:
    period = OrcFxAPI.SpecifiedPeriod(time, time)
    LiftLineTension = winch.TimeHistory('Tension', period)[0]
    print time, LiftLineTension

    if LiftLineTension > MaxTension:
        MaxTension = LiftLineTension
    if LiftLineTension < MinTension:
        MinTension = LiftLineTension

ws1.write(Casenumber, 0, Casenumber)
ws1.write(Casenumber, 1, Direction)
ws1.write(Casenumber, 2, Hs)
ws1.write(Casenumber, 3, Tz)
ws1.write(Casenumber, 4, MaxTension)
ws1.write(Casenumber, 5, MinTension)
wb.save('C:\Users\Rbjerkholt\Documents\Skole\Master\Orcaflex\Master\ROVlifting\
    AllSeaStates ROV 2\Lifting\ResultLiftLineTensionSeed3_12s.xls')
```

F Results from OrcaFlex

F.1 Operational Limit for Launching, ROV model 1

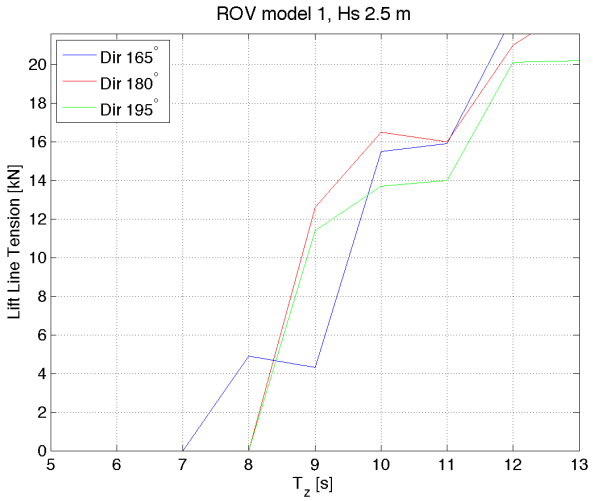

Figure F.1: Minimum tension, Hs 2.5 m

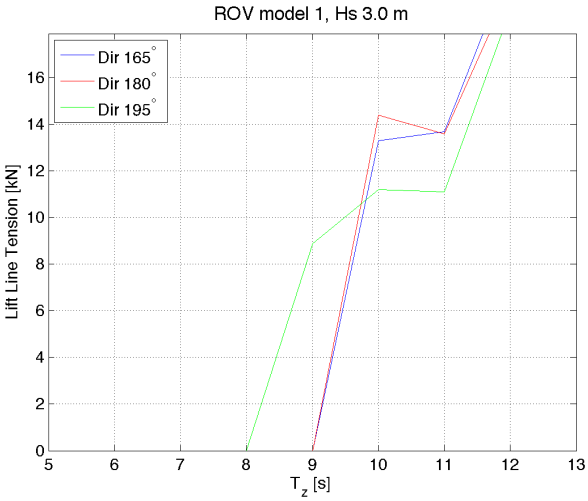

Figure F.2: Minimum tension, Hs 3.0 m

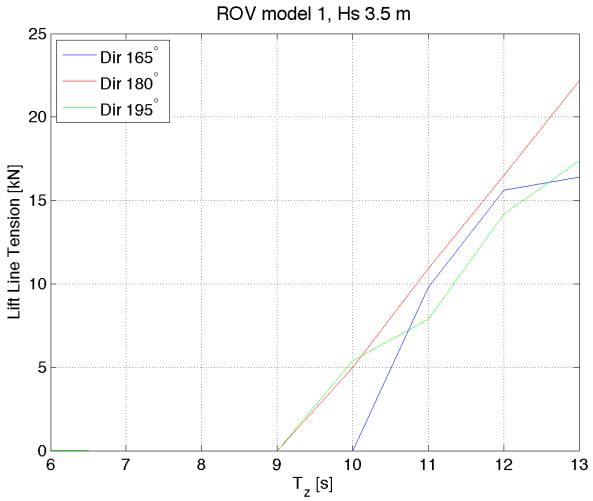

Figure F.3: , Minimum tensionHs 3.5 m

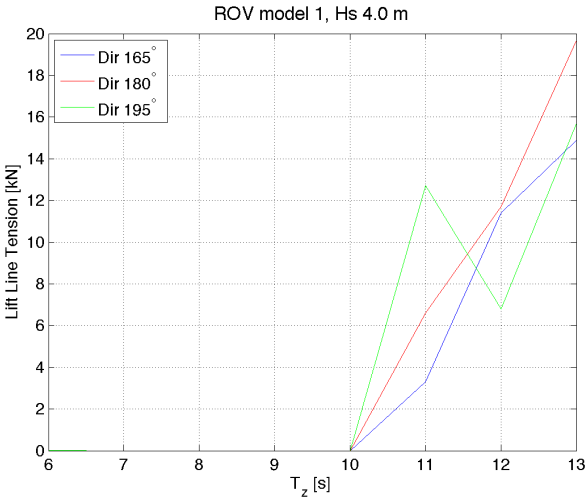

Figure F.4: Minimum tension, Hs 4.0 m

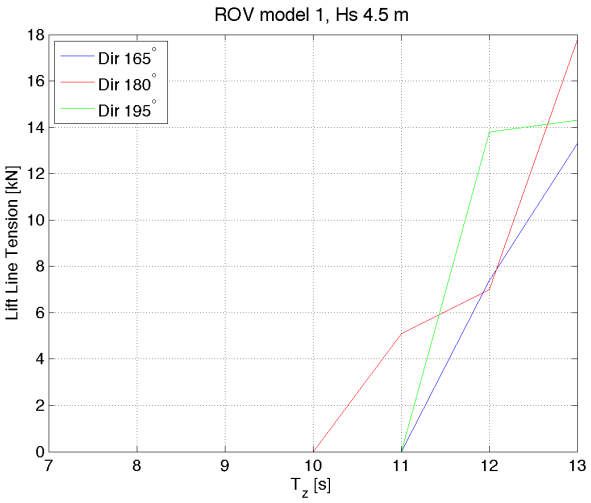

Figure F.5: Minimum tension, Hs 4.5 m

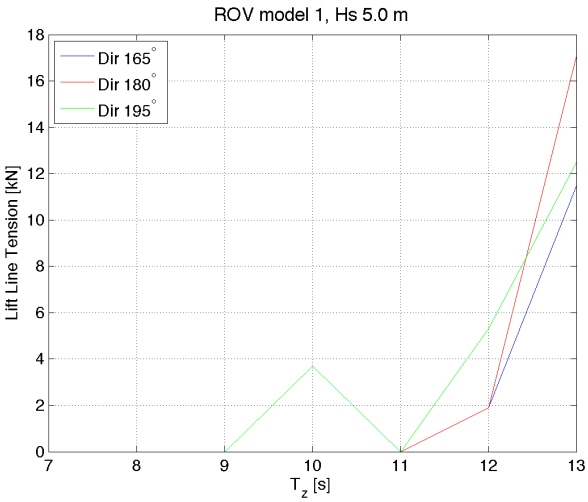

Figure F.6: Minimum tension, Hs 5.0 m

F.2 Operational Limit for Launching, ROV model 2

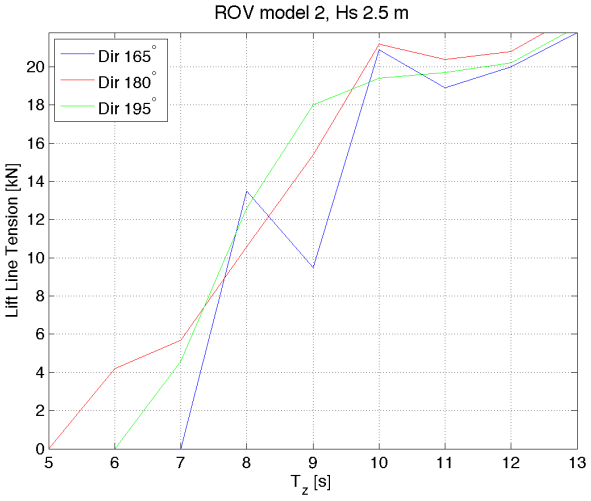

Figure F.7: Minimum tension, Hs 2.5 m

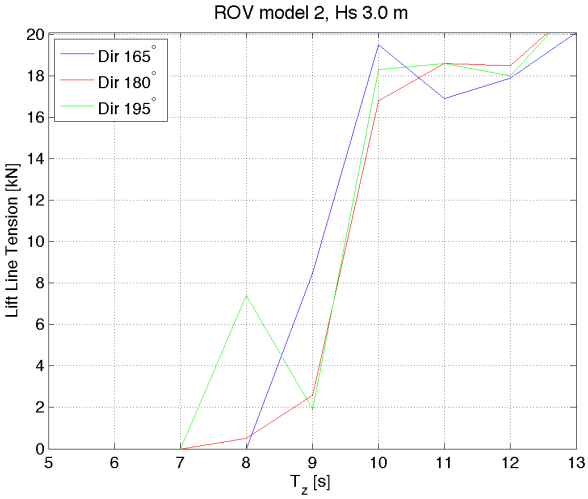

Figure F.8: Minimum tension, Hs 3.0 m

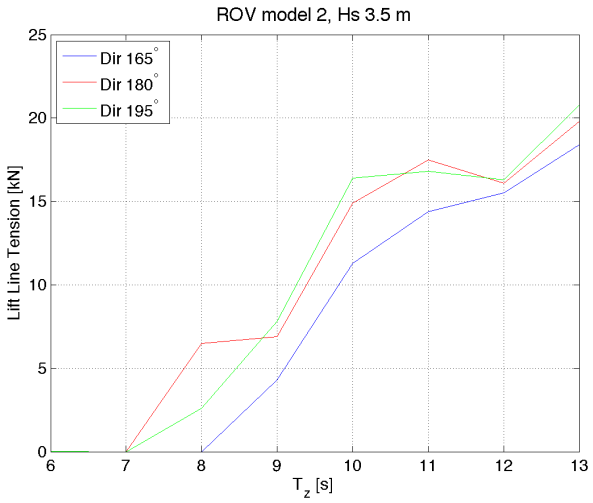

Figure F.9: Minimum tension, Hs 3.5 m

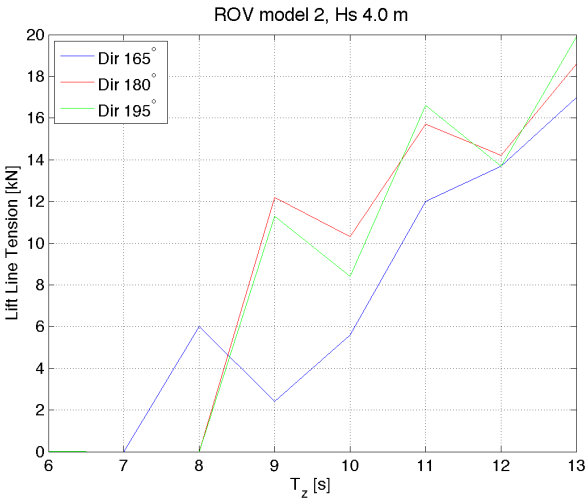

Figure F.10: Minimum tension, Hs 4.0 m

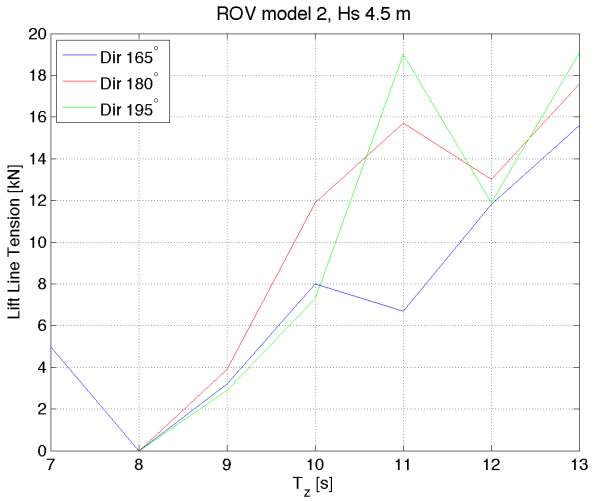

Figure F.11: Minimum tension, Hs 4.5 m

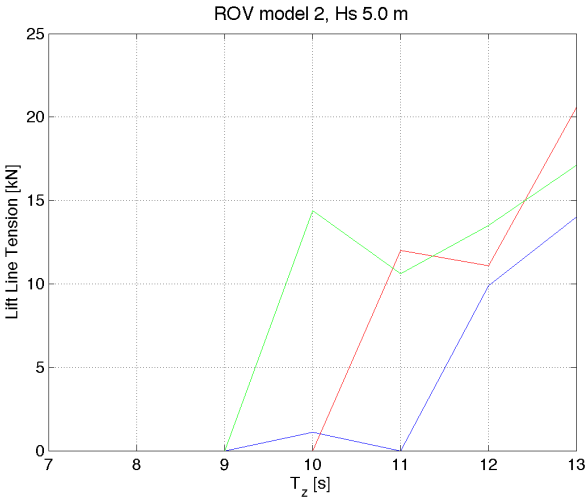

Figure F.12: Minimum tension, Hs 5.0 m

F.3 Operational Limit for Recovery, ROV model 1

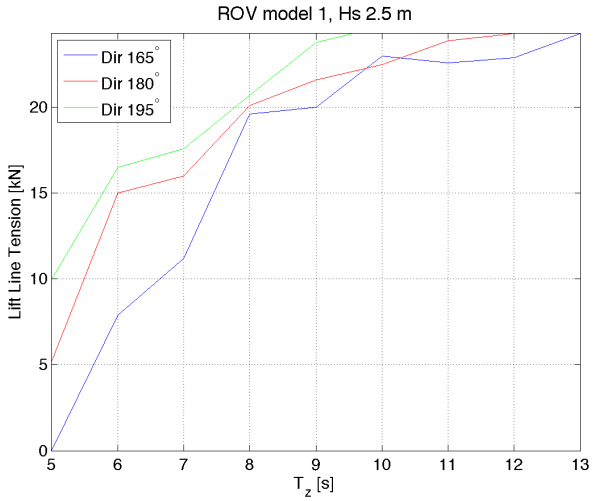

Figure F.13: Minimum tension, Hs 2.5 m

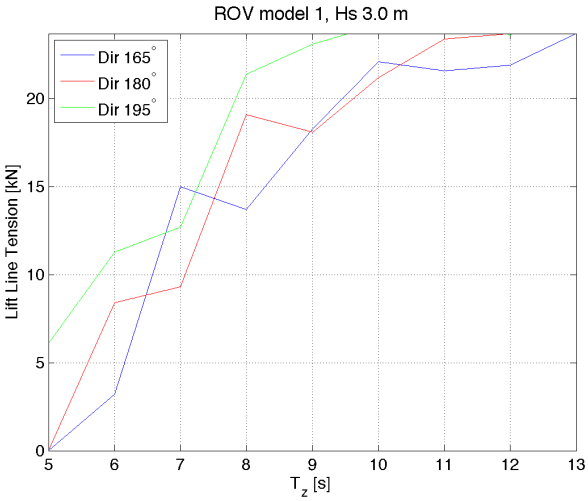

Figure F.14: Minimum tension, Hs 3.0 m

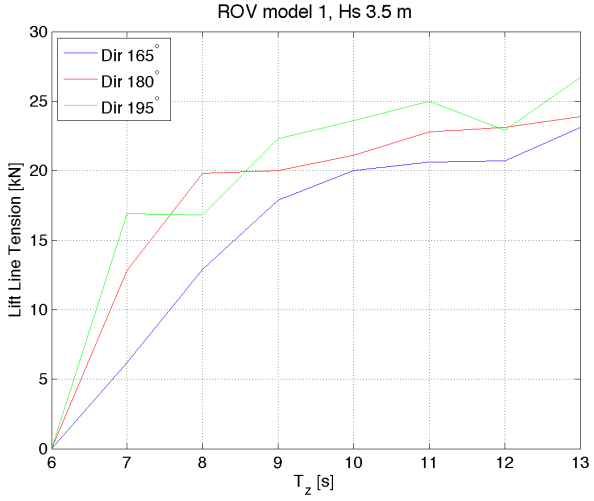

Figure F.15: Minimum tension, Hs 3.5 m

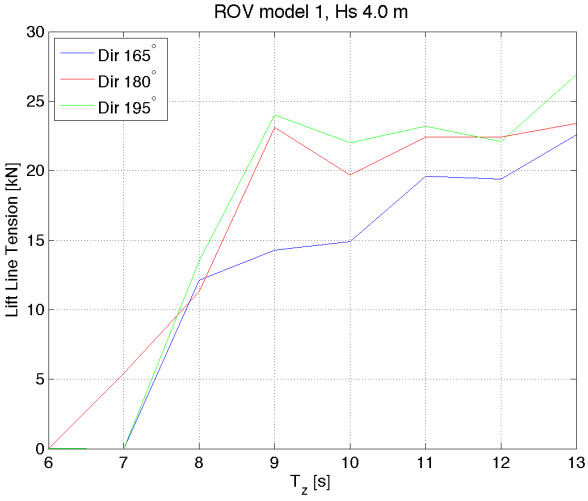

Figure F.16: Minimum tension, Hs 4.0 m

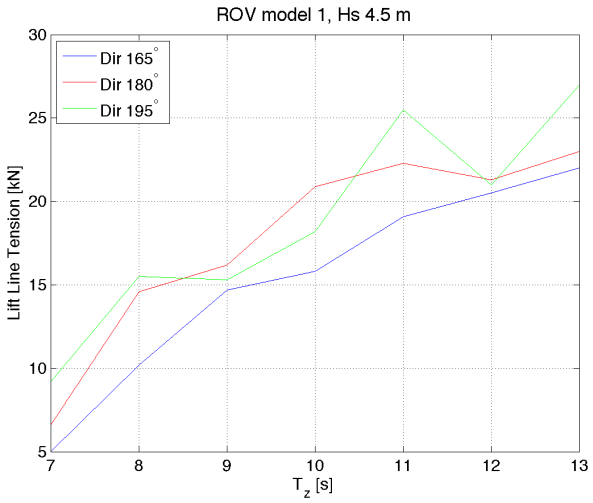

Figure F.17: Minimum tension, Hs 4.5 m

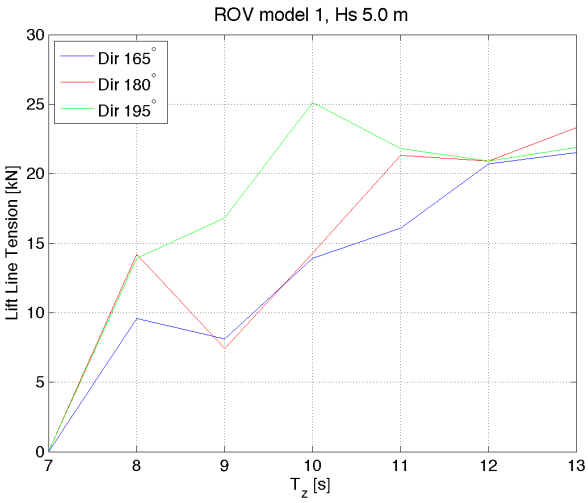

Figure F.18: Minimum tension, Hs 5.0 m

F.4 Operational Limit for Recovery, ROV model 2

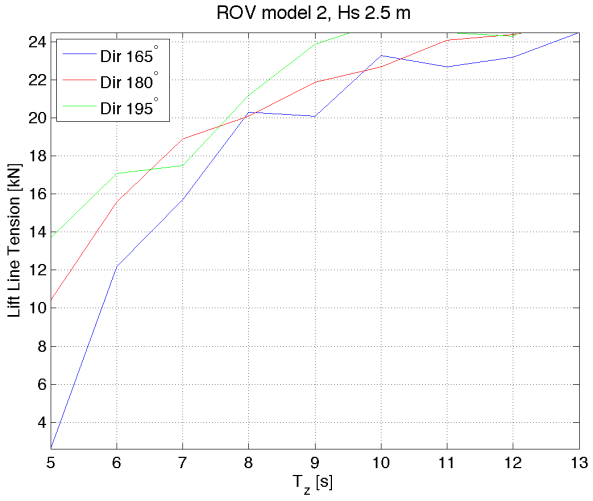

Figure F.19: Minimum tension, Hs 2.5 m

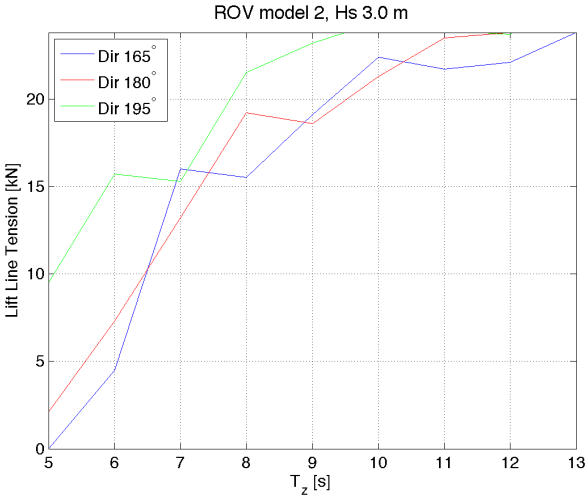

Figure F.20: Minimum tension,, Hs 3.0 m

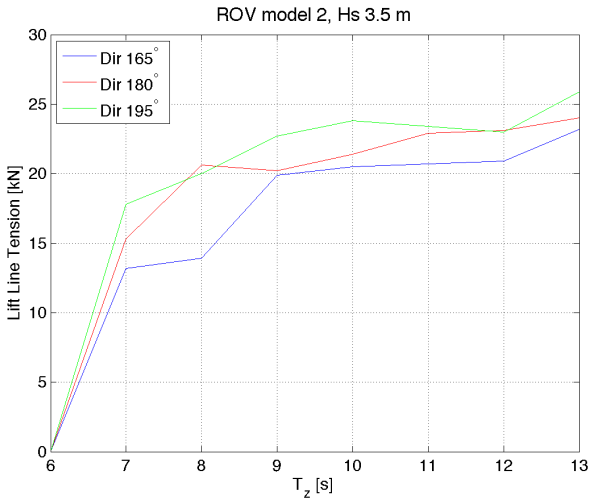

Figure F.21: Minimum tension, Hs 3.5 m

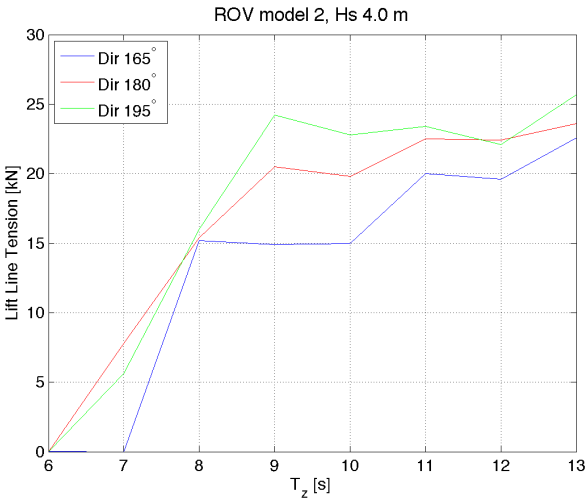

Figure F.22: Minimum tension, Hs 4.0 m

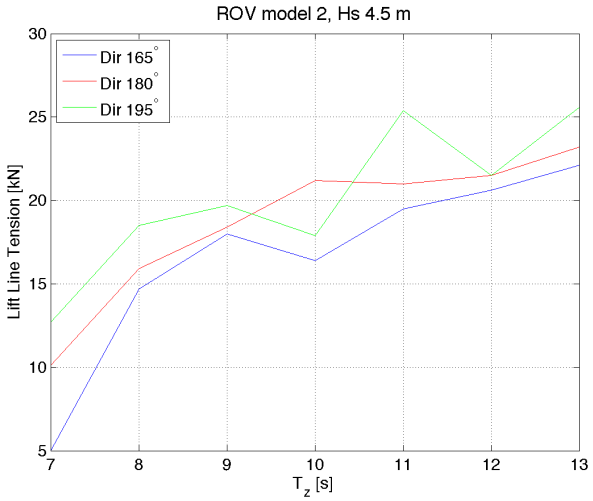

Figure F.23: Minimum tension, Hs 4.5 m

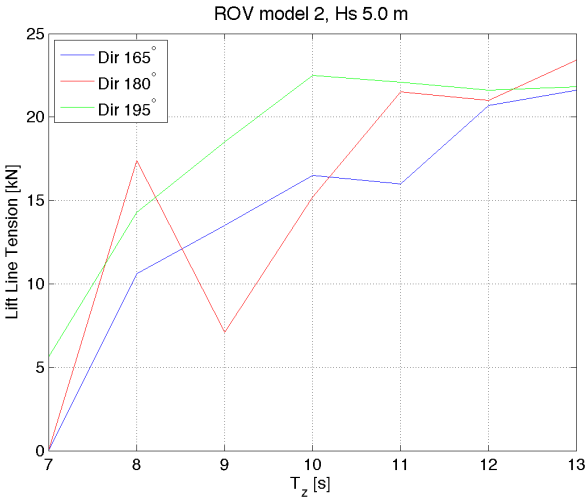

Figure F.24: Minimum tension, Hs 5.0 m